

The red supergiant population in the Perseus arm

R. Dorda,¹[★] I. Negueruela¹ and C. González-Fernández²

¹*Departamento de Física, Ingeniería de Sistemas y Teoría de la Señal, Universidad de Alicante, Carretera de San Vicente s/n, San Vicente del Raspeig E03690, Alicante, Spain*

²*Institute of Astronomy, University of Cambridge, Madingley Road, Cambridge CB3 0HA, United Kingdom*

Accepted XXX. Received YYY; in original form ZZZ

ABSTRACT

We present a new catalogue of cool supergiants in a section of the Perseus arm, most of which had not been previously identified. To generate it, we have used a set of well-defined photometric criteria to select a large number of candidates (637) that were later observed at intermediate resolution in the the Infrared Calcium Triplet spectral range, using a long-slit spectrograph. To separate red supergiants from luminous red giants, we used a statistical method, developed in previous works and improved in the present paper. We present a method to assign probabilities of being a red supergiant to a given spectrum and use the properties of a population to generate clean samples, without contamination from lower-luminosity stars. We compare our identification with a classification done using classical criteria and discuss their respective efficiencies and contaminations as identification methods. We confirm that our method is as efficient at finding supergiants as the best classical methods, but with a far lower contamination by red giants than any other method. The result is a catalogue with 197 cool supergiants, 191 of which did not appear in previous lists of red supergiants. This is the largest coherent catalogue of cool supergiants in the Galaxy.

Key words: (stars:) supergiants – stars: massive – stars: late-type – (Galaxy:) open clusters and associations: general – Galaxy: stellar content

1 INTRODUCTION

The section of the Perseus arm visible from the Northern hemisphere is a Galactic region rich in young stars, with many OB associations and young open clusters (Humphreys 1978). Given its proximity to the Sun (with typical distances ranging between 3 kpc at $l \sim 100^\circ$ to 2 kpc at $l \sim 140^\circ$; Choi et al. 2014), it offers important advantages for the study of stellar populations over other Galactic regions. Located towards the outskirts of the Milky Way, it presents a moderately low reddening, which makes young blue stars easily accessible. In consequence, the high-mass population in Perseus has been widely studied for decades (e.g. Humphreys 1978). Among the young stars in Perseus, there are also many red supergiant (RSG) stars (> 70 ; Humphreys 1978; Levesque et al. 2005). These stars possess moderately-high mass (~ 10 to $\sim 40 M_\odot$), high luminosity ($\log(L/L_\odot) \sim 4.5 - 5.8$; Humphreys & Davidson 1979), low temperature¹, and late (K or M) spectral type (SpT). Although they have

evolved off the main sequence, RSGs are still young stars (with ages between ~ 8 and ~ 25 Ma; Ekström et al. 2013). In consequence, they are associated to regions of recent stellar formation.

The correct characterisation of the RSG phase plays a major role in the understanding of the evolution and final fate of high-mass stars (e.g. Ekström et al. 2013). Despite this pivotal position, there are still many critical questions about them that remain without definitive answers; among them, the definition of a temperature scale and its relation with luminosity, as discussed in Dorda et al. (2016a, from now on Paper II). To bring some light to these questions, we started an ambitious observational programme on RSGs, aimed at characterising their properties by using statistically significant samples. In González-Fernández et al. (2015, from now on, Paper I) we presented the largest spectroscopic sample to date of cool supergiants² (CSGs) from the

ent temperature ranges. In all cases, though, the effective temperatures of these stars are well below 4500 K.

² "Cool supergiants" is a denomination that includes all red and some yellow supergiants. In Paper I, we showed that G-type SGs in the SMC (and presumably other low-metallicity environments) are part of the the same population as RSGs. This is not the

[★] E-mail: ricardo.dorda@ua.es

¹ The temperature scale of RSGs is still an open question. Over the last decade, different works (Levesque et al. 2007, Davies et al. 2013, and Tabernero et al. submitted) have reported quite differ-

Magellanic Clouds (MCs). By combining this large sample with an important number of well-characterised Milky Way RSGs, in [Paper II](#) we could present firm statistical confirmation of a correlation between SpT and temperature, or the relation between SpT, luminosity, and mass loss. Taking advantage of this sample, in [Dorda et al. \(2016b, Paper III\)](#) we developed an automated method for the identification of CSGs using the atomic and molecular features in the spectral range around the infrared Calcium Triplet (CaT). Finally, Tabernero et al. (submitted) have calculated the effective temperatures for the sample in [Paper I](#) and studied the temperature scales of the RSGs from the MCs.

The present work is the next step in our study of CSGs. After analysing the CSG population from the MCs, we extend our study to the Milky Way population of CSGs. As many of the properties of a given CSG population (e.g. its typical SpT and temperatures) depend on its metallicity ([Elias et al. 1985](#)), we selected a specific region of the Galaxy where we can expect rather uniform (typically solar) metallicities: the section of the Perseus arm between $l = 97^\circ$ and 150° , with Galactocentric distances in the ~ 8 to 10 kpc range. This region was chosen because of the many RSGs that were previously known and well characterised, but also because its CSGs have very low apparent magnitudes and can be observed efficiently with long-slit spectrographs. A systematic search for CSGs in an area that is considered well studied allows a good estimation of the incompleteness of previous samples. Moreover, as the extinction towards the Perseus arm is relatively low, its blue population is well known. In consequence, the relation between OB stars and CSGs can be studied. This analysis would be specially interesting, because many clusters and OB associations in the Perseus arm have total masses and ages coherent with the presence of CSGs.

In this paper, we apply the methods developed in [Paper III](#) to a sample of candidate RSGs from the Perseus arm, to test their reliability and obtain a statistically significant sample of CSGs in the area. In addition, we develop a method to compute the likelihood that a given star is indeed a supergiant and estimate the reliability of our identification. We also study some basic properties of the CSG population at solar metallicities, such as its SpT distribution and its relation with the luminosity class (LC). In a future work, we will carry out a deeper study of the astrophysical properties of the the CSG sample found here, analysing its spatial and kinematic distributions, as well as its connection to the known population of high-mass stars close to the main sequence.

case in the Milky Way, but a few luminous G-type supergiants are part of our calibration sample. Thus, we use the term CSG to make reference to the present sample. Despite this, the term RSG is used in many cases, in reference to the samples of K and M supergiants studied in previous works (e.g. [Humphreys 1978](#); [Levesque et al. 2005](#)).

2 OBSERVATIONS AND MEASUREMENTS

2.1 Target selection

To identify RSG candidates in the Perseus arm, we performed a comprehensive photometric search in the Galactic Plane ($b = +6^\circ$ to -6° , and $l = 97^\circ$ to 150°). We used as a guide the works of [Humphreys \(1970, 1978\)](#). The selection is the result of the following steps:

- From [Humphreys \(1978\)](#) we selected those regions with detected RSGs and distance moduli (DM) coherent with being part of the Perseus arm.
- Using these DM, along with the measured A_V , we selected from 2MASS those sources with K band magnitudes bright enough to be a RSG, assuming a lower limit for their intrinsic brightness at $M_K = -5$. This may seem a very low limit, as for example in [Paper I](#) there are no CSGs below $M_K \sim -7$, but it allows for large errors in DM and/or extinction while keeping the CSG candidate sample as complete as possible. This step gets rid of most of the foreground and background undesired populations, as the expected density profile of the Galaxy along this line of sight allows us to adopt a low luminosity threshold without risking too much contamination (more distant RSGs will likely be also included, but they are expected to be rare in the outer reaches of the Galaxy and will be of interest for future studies). This leaves only nearby dwarfs and giants with types later than M3 as main interlopers.
- The filtered sample was then cross-correlated with well known catalogues of optical photometry, such as USNO-B1 ([Monet et al. 2003](#)) and UCAC3 ([Zacharias et al. 2010](#)), obtaining I band magnitudes and proper motions. Candidates are required to have $(I - K_S)_0 > 2$ (roughly, the colour of a K0 star) and proper motions similar to those of the blue and red supergiants already known in the field. This step cleans the sample of most of the foreground stars, as they have higher motions.
- The remaining catalogue was then submitted to SIMBAD and all the stars with confirmed SpTs were removed, although we kept 51 previously-studied RSGs, for a number of reasons: check spectral variations, test the efficiency of our methods and provide a comparison sample. In fact, 43 of these objects with reliable SpT or marked as MK standards were used for the calibration sample used in [Paper III](#). In consequence, we are not considering these 43 SGs as part of the test sample, but we include them to calculate the efficiency of the photometric selection in [Sect. 4.2](#).

2.2 Observations

The targets were observed during two different campaigns. The first one was done in 2011, on the nights of October 16th, 17th, and 18th. The second campaign was carried out in 2012, from September 3rd to 7th. We used the Intermediate Dispersion Spectrograph (IDS), mounted on the 2.5 m Isaac Newton Telescope (INT) in La Palma (Spain). We used the *Red+2* CCD with its 4096-pixel axis along the wavelength direction. The grating employed was R1200R, which covers an unvignetted spectral range 572 \AA wide, centred on 8500 \AA (i.e. the spectral region around the infrared Calcium Triplet, CaT). This configuration, together with a slit width of $1''$, provides a resolving power of $R \sim 10\,500$ in the spec-

tral region observed. This R is very similar to the resolution of the data used in [Paper I](#) ($R \sim 11\,000$). The reduction was carried out in the standard manner, using the IRAF facility³.

In total, we observed 637 unique targets, 102 in 2011 and 535 in 2012, without any overlap between epochs. As discussed above, 43 of them are CSGs with well determined SpTs (all but one observed in the 2012 run) that were included in the calibration sample of [Paper III](#) (see appendix B in that work). These objects are not considered part of the Perseus sample studied here. This leaves 594 targets in our sample, which are detailed in Table A1.

2.3 Manual classification and spectral measurements

We performed a visual classification for all the stars in the sample, using the classical criteria for the CaT spectral region explained in [Negueruela et al. \(2012\)](#). All the carbon stars found (46) were marked and removed from later calculations. Thus, we do not use them in the present work, but they are included in our complete catalogue (see Table A1). Without the carbon stars, our sample has 548 targets.

For the analysis of our sample, we used the principal component analysis (PCA) method described in [Paper III](#). This method begins with the automated measurement of the main spectral features in the CaT spectral region. We measured all the features needed to calculate the principal components (PCs) of our stars (i.e. those marked as shortened input list in table C.1 from [Paper III](#)). The method to measure these features is the same as for the calibration sample in [Paper III](#). Although the resolution of our sample is not exactly the same as in the calibration sample, it is close enough not to introduce any significant difference in the result, as explained in [Paper III](#).

Finally we combined linearly the PCA coefficients (tables D.1 and D.2 in [Paper III](#)) with the spectral measurements of each star in our sample, obtaining their corresponding PCs. We also calculated their uncertainties, propagating the uncertainties of the EWs and PC coefficients through a lineal combination.

3 ANALYSIS

3.1 Estimating the probability of being a CSG

In [Paper III](#) we revisited the main criteria classically used to identify RSGs, discussing the advantages and limitations of each one. We also proposed an original method, based on the PCs calculated through a large calibration sample and the use of Support Vector Machines (SVM). All the classical criteria, as well as the PCA method, use boundaries between the SGs and non-SGs as separators (our method uses many boundaries in a multidimensional space, but it is qualitatively the same in concept). Thus, they provide a binary classification for the targets (each of them is classified

as either SG or non-SG), but without any direct estimation of the reliability of their classifications.

In [Paper III](#) we also defined two useful concepts for our analysis: efficiency and contamination. Efficiency is the fraction of all SGs that is identified as such by a given criterion, while contamination is the fraction of the stars selected as SGs by a given criterion that are not really SGs. Efficiencies and contaminations obtained for the calibration sample are based on the statistics of the whole sample, and give a good idea of the reliability of each method when it is applied to a large number of candidates. However, it is not a good measurement of the reliability of the individual classification of each target: the result is the same for a star that lies close to the boundary as for one that is far away from it. In consequence, we wanted to measure the reliability of each individual identification. For this, we used a Montecarlo process that delivers the individual probability of each target being a SG ($P(\text{SG})$). We detail the process and the results for the calibration sample in the following Section 3.1.1. Later, after testing the method in the calibration sample, we calculate the probabilities for the test sample of this work in Section 3.2.

3.1.1 Calculation

For each one of the three classification methods described in the following paragraph, we obtained uncertainties through a Montecarlo process using each target in the calibration sample from [Paper III](#). We took the variables needed for each method and their errors, and we drew a new value for the variable from a random normal distribution, with the original measurement as centre and the error as its standard deviation. For each target, we sampled 1000 draws, and so we obtained 1000 different sets of derived variables. To these we applied the corresponding classification methods, and checked how many times the target was classified as a SG or not in each draw. The $P(\text{SG})_{\text{method}}$ of a target is the fraction of realizations which resulted in a positive identification.

For what we call the PCA method ($P(\text{SG})_{\text{PCA}}$), we used the first 15 PCs (which contain 98% of the accumulated variance), and the SVM calculation defined in [Paper III](#) (using a putative boundary at M0; see [Paper III](#)), obtaining the $P(\text{SG})_{\text{PCA}}$ for each target. The results of this procedure are shown in Fig. 1. We also calculated the $P(\text{SG})_{\text{CaT}}$ for the criterium based on the strength of the CaT (a target is identified as a SG if the sum of the EWs of its three Ca lines is equal to or higher than $9\,\text{\AA}$), and $P(\text{SG})_{\text{Ti/Fe}}$ for the Ti/Fe method (which uses as boundary the line $\text{EW}(8514.1) = 0.37 \cdot \text{EW}(8518.1) + 0.388$ in the Fe I 8514 \AA vs. Ti I 8518 \AA diagram). The results are shown in Figs. 2 and 3. The other classical criteria considered in [Paper III](#), based on the strength of the blend at 8468 \AA and the EWs of only the two strongest lines of the CaT, have been not used here because of their low efficiency or high contamination.

3.1.2 Identification based on individual probabilities

With the classical criteria studied, based on the CaT and on the Ti/Fe ratio, a large fraction of the SGs (> 0.85 and > 0.70) in the sample have $P(\text{SG}) = 1$ and most non-SGs

³ IRAF is distributed by the National Optical Astronomy Observatories, which are operated by the Association of Universities for Research in Astronomy, Inc., under cooperative agreement with the National Science Foundation

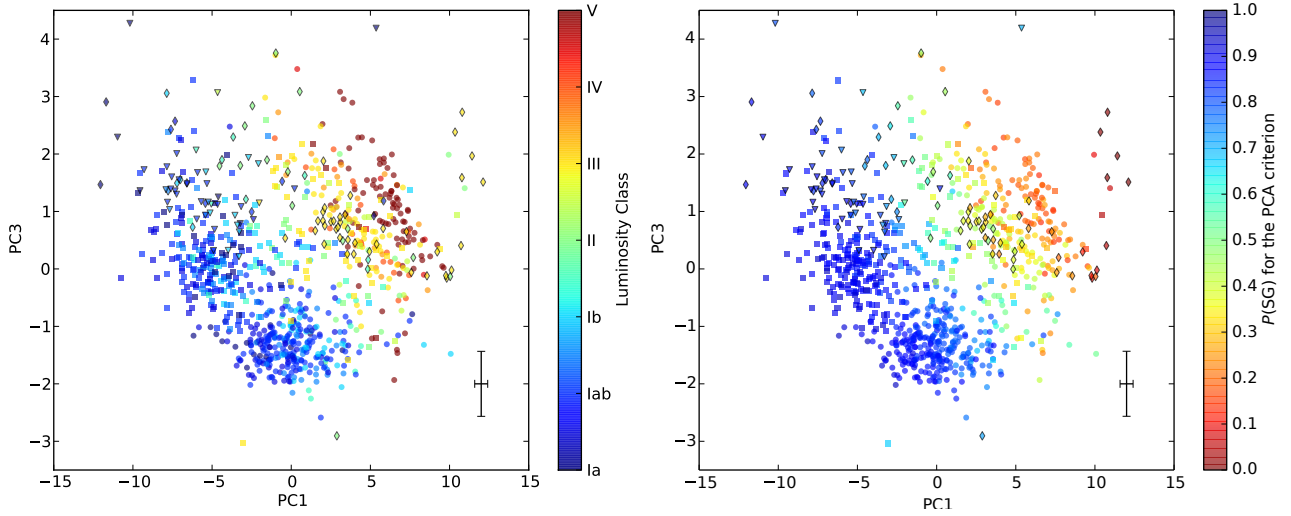


Figure 1. PC1 versus PC3 diagram for the calibration sample. The shapes indicate their origin: circles are from the SMC survey, squares are from the LMC survey, diamonds are Galactic standard stars, and inverted triangles are the stars from the Perseus arm survey used as part of the calibration sample (see Section 2.3). The cross indicates the median uncertainties, which have been calculated by propagating the uncertainties through the linear combination of the input data (EWs and bandheads) with the coefficients calculated in Paper III. **Left (1a):** The colour indicates LC (identical to figure 7b in Paper III). **Right (1b):** The colour indicates the probability of being a SG (see 3.1.1).

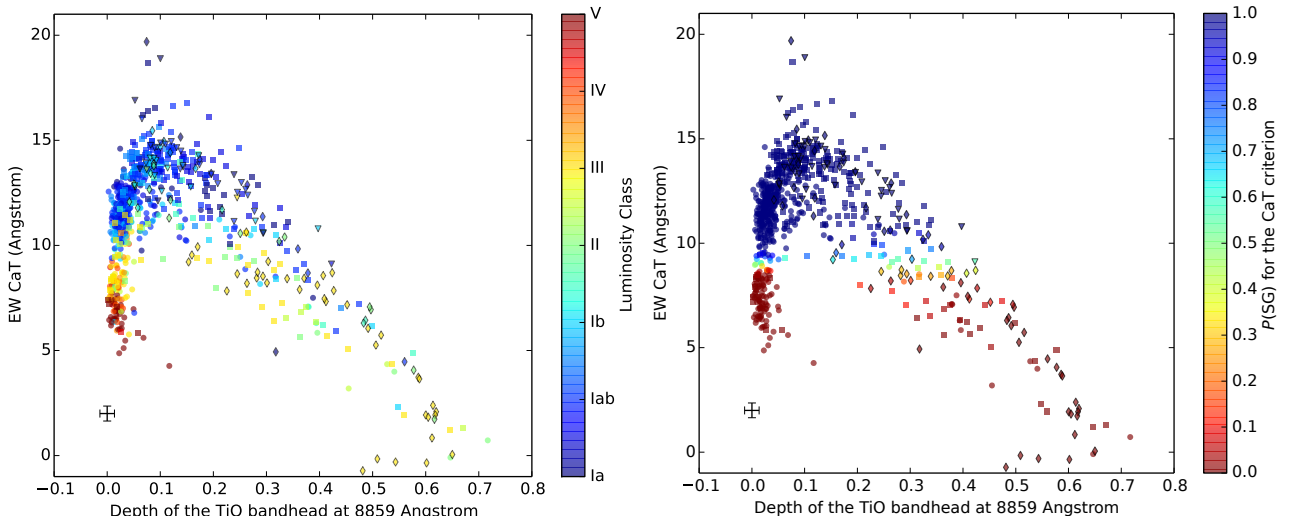


Figure 2. Depth of TiO bandhead at 8859 Å versus total equivalent width of the Calcium Triplet (8498 Å, 8542 Å, and 8662 Å), for the calibration sample. The strength of the TiO 8859 Å bandhead is simply an indicator of the spectral sequence for early to mid-M stars (see Section 4.3.4 in Paper III) and is included here simply to display the measurements in a 2D graphs, so that the CaT criterion is easily visualised. Symbol shapes are the same as in Fig. 1. The black cross indicates the median uncertainties. In these panels the probability of being a SG (see 3.1) can be compared to the actual LC classification. **Left (2a):** The colour indicates LC. **Right (2b):** The colour indicates the probability of being a SG (see 3.1.1).

have $P(\text{SG}) = 0$. Only those stars close to the boundary used by these methods present intermediate values of $P(\text{SG})$. Since the boundaries between SGs and non-SGs in these diagrams are straight lines, a given star can be identified as a SG if it has $P(\text{SG}) \geq 0.5$ – this is equivalent to the simple assignment to one of the two categories. On the other hand, in the PCA method there are not many targets with their $P(\text{SG})$ equal to 1 or to 0. This is because the PCA uses many boundaries in the multidimensional space of the PCs, not a single boundary in a two dimensional diagram, as is the case of the classic criteria. Thus it is more difficult to stay

far away from every boundary and the probabilities tend to have intermediate values.

To illustrate this, and also to evaluate the application of this method to the identification of SGs, we calculated how many targets have their individual probability P_i equal to or higher than a given $P(\text{SG})$ value. As the SGs from each galaxy in the calibration sample have different typical SpTs (Levesque 2013; Paper II), we performed this calculation for six different subsamples taken from the calibration sample: SGs from the SMC, from the LMC, from the MW, all SGs, all non-SGs, and the whole sample. We present the results

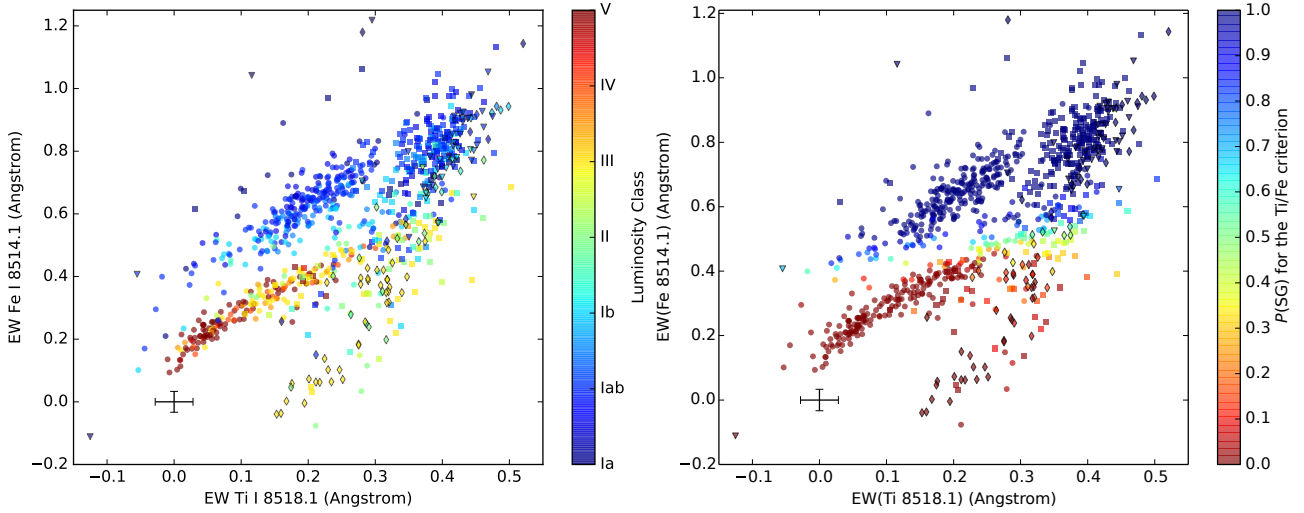


Figure 3. EWs of the lines Fe I 8514 Å and Ti I 8518 Å for the calibration sample. Symbol shapes are the same as in Fig. 1. The cross indicates the median uncertainties. In these panels the probability of being a SG (see 3.1) can be compared with the actual LC classification. **Left (2a):** The colour indicates LC (Equivalent to Fig. 12b from Paper III). **Right (2b):** The colour indicates the probability of being a SG (see 3.1.1).

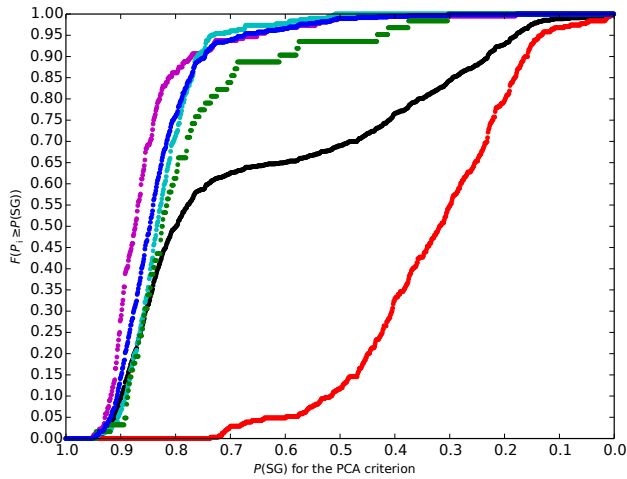


Figure 4. Fraction of the calibration sample that has a probability of being a SG (calculated through the PCA method) equal to or higher than the corresponding x-axis value. The colours indicate the subsample: black for whole sample, red for non-SGs, blue for all SGs, magenta for SMC SGs, cyan for LMC SGs, and green for MW SGs. Each fraction is calculated with respect to the size of its own subsample.

for each of these subsamples as fractions ($F(P_i \geq P(\text{SG}))$) with respect to their corresponding total size, in Figs. 4, 5, and 6. For all three classification criteria, the SGs from both MCs present very similar behaviours, but the SGs from the MW present slightly lower probabilities. This small difference is likely due to the lower efficiency of all criteria towards later subtypes, as it is well known that SGs in the MW tend to have later subtypes than those in the MCs (Levesque 2013).

The CaT and the Ti/Fe criteria result in a large fraction of SGs with high values of $P(\text{SG})$, but there are non-SGs with probabilities as high as $P(\text{SG}) = 1$. Thus, these methods

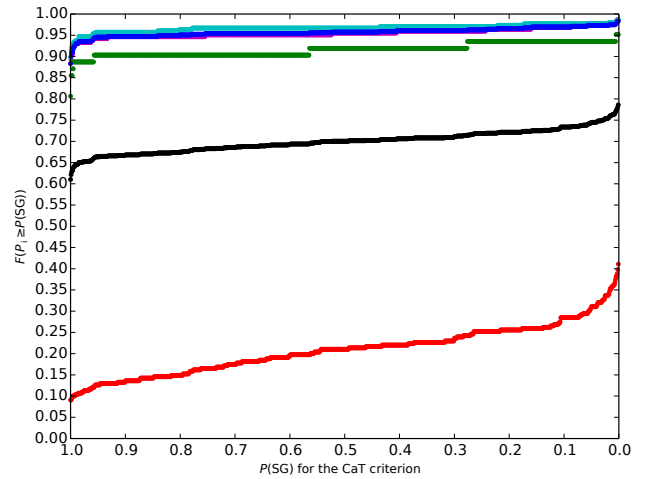


Figure 5. Fraction of the calibration sample that has a probability of being a SG (calculated through the CaT method) equal to or higher than the corresponding x-axis value. The colours indicate the subsample, as explained in Fig. 4. Each fraction is calculated with respect to the size of its own subsample.

provide a quick way to identify most SGs in the sample, but at the price of having a significant contamination. Of these two methods, the CaT one is less strict, finding more SGs, but also including more non-SGs with high $P(\text{SG})$ values.

The PCA method finds a very small fraction of SGs with $P(\text{SG}) > 0.9$ (and this fraction is significantly higher for SMC SGs than for MW ones, as can be seen in Fig. 4). However, non-SGs present significantly lower values of $P(\text{SG})$, with none of them having $P(\text{SG}) > 0.75$. For this value the fraction of SGs identified is about 0.90 ± 0.04 ($\sim 0.80 \pm 0.13$ for the SGs from the MW). Therefore, using this value as a threshold, the vast majority of SGs can be identified without any contamination. In addition, it is also possible to identify a group of likely SGs with a relatively low contamination,

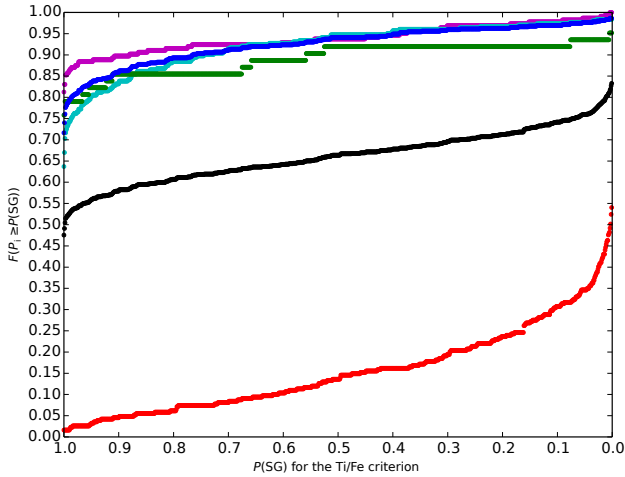


Figure 6. Fraction of the calibration sample that has a probability of being a SG (calculated through the ratio of the Fe I 8514 Å to Ti I 8518 Å lines) equal to or higher than the corresponding x -axis value. The colours indicate the subsample, as explained in Fig. 4. Each fraction is calculated with respect to the size of its own subsample.

by taking the targets whose $P(\text{SG})$ lies within the interval between $P(\text{SG}) = 0.75$ and a lower limit set at convenience (depending on the level of contamination that may be considered acceptable).

For a new sample, such as the Perseus arm sample in this paper, it is possible to estimate the value of this lower limit of $P(\text{SG})$ that results in an optimal selection of potential SGs. In such a sample, the only information available will be the shape of the $P(\text{SG})$ fraction curve (the black line in our figures). This curve, however, will always have an inflexion point at the $P(\text{SG})$ value where most SGs have already been selected, while most non-SGs have lower values of $P(\text{SG})$. Thus, from this point towards lower probabilities, the addition of extra targets to the selection becomes dominated by non-SGs. Therefore, this inflexion point can be used as a lower boundary for the group of potential SGs, and can be easily estimated for any sample under study, as we do for the Perseus sample in next Section.

In the calibration sample, the inflexion point is at $P(\text{SG}) \sim 0.60$. Taking this value as a lower boundary, the efficiency of the resultant selection is higher than 0.95 ± 0.04 ($\sim 0.90 \pm 0.13$ for SGs from the MW), while the contamination is only 0.03 ± 0.04 (0.08 ± 0.13 in the case of the MW sample). Note that the contaminations were calculated for the total number of stars tagged as SGs, i.e. all those having $P(\text{SG}) \geq 0.60$. For similar efficiencies in the CaT and Ti/Fe ratio criteria, the contaminations are slightly higher ($\sim 0.08 \pm 0.04$ in both cases). These values become slightly worse in the case of MW SGs, with contaminations of 0.17 ± 0.13 for the Ti/Fe ratio criterion and 0.20 ± 0.13 for the CaT one. In Paper III we found that the PCA method provides a higher quality method to identify SGs than the other two, because it has a significantly lower contamination. In this work, we found another advantage: the possibility to identify a large fraction of SGs without any contamination.

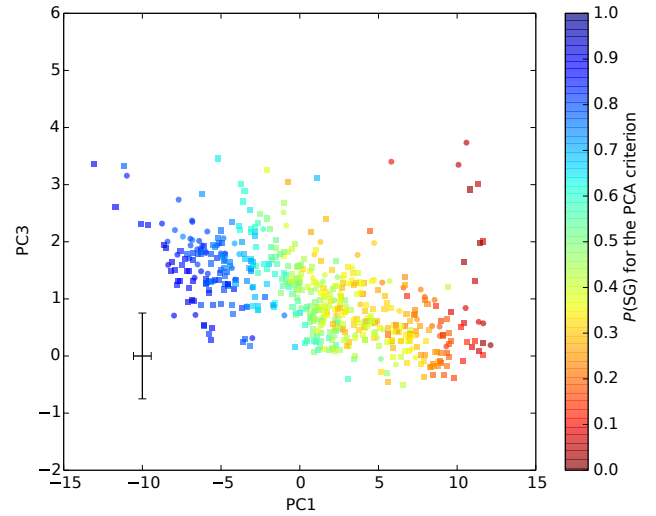


Figure 7. PC1 versus PC3 diagram for the Perseus sample. The shapes indicate epoch: 2011 circles, 2012 squares. The black cross indicates the median uncertainties, which have been calculated by propagating the uncertainties through the linear combination of the input data (EWs and bandheads) with the coefficients calculated. The colour indicates $P(\text{SG})_{\text{PCA}}$. The plot is shown at the same scale as Fig. 1, to ease comparison. The differences in the target distribution with respect to the calibration sample are due to the different ranges of spectral types.

3.2 Probabilities for the Perseus sample

Before the analysis of our Perseus sample, we must stress that the SGs from the MW typically have M subtypes. We may thus expect our sample to be dominated by these subtypes. Moreover, most of the interlopers found in the manual classification are red giants with M types. In consequence, the diagrams obtained for the Perseus sample have their datapoints concentrated in the regions typical of M-type stars, and look quite different from the distributions seen in the calibration sample (see Figs. 1, 2, and 3), whose SpT range spans from G0 till late-M subtypes. For further details about the calibration sample and their SpT distribution, see Paper III and figs. 7a, 9, and 12a therein.

We calculated the individual probabilities of being a SG for each target in the Perseus sample, following the same method described for the calibration sample (Section 3.1). Using the PCs previously obtained for our targets, $P(\text{SG})_{\text{PCA}}$ was calculated through a Montecarlo process (generating 1000 new sets of PCs per target). The results are given in Table A1 and represented in a PC1 to PC3 diagram in Fig. 7.

Although the PCA method provides significantly better results than classical criteria, we also calculated the probabilities for them (CaT and Ti/Fe). We include these criteria because they are useful for a quick estimate despite their limitations. In addition, this is the first time that these criteria are systematically applied them to a very large sample at solar metallicity: more than 500 targets, instead of the ~ 100 MW stars from the calibration sample. The results are given in Table A1, and presented in Figs. 9 and 10.

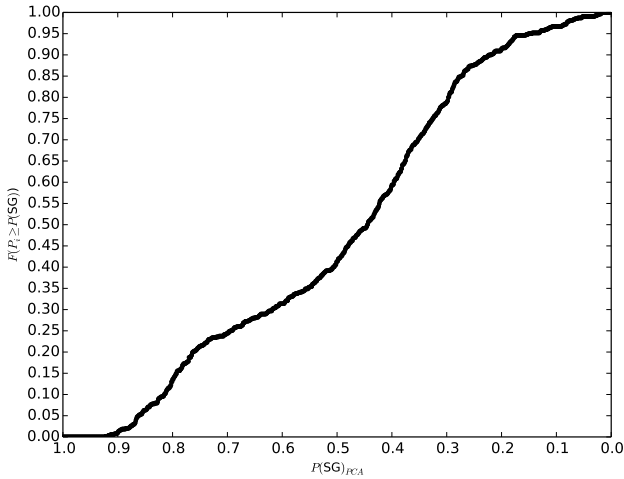


Figure 8. Fraction of the Perseus sample that has a probability of being a SG (calculated through the PCA method) equal to or higher than the corresponding x -axis value.

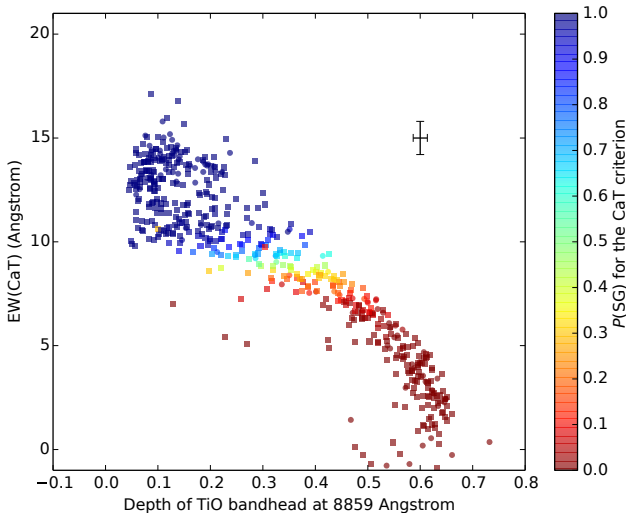


Figure 9. Depth of the TiO bandhead at 8859 Å with respect to the sum of the EWs of the CaT lines. The shapes indicate epoch: 2011 circles, 2012 squares. The black cross indicates the median uncertainties. The colour indicates $P(\text{SG})_{\text{CaT}}$. Note again the difference in SpT distribution with respect to the calibration sample (Fig. 2).

4 RESULTS

4.1 Supergiants identified

When we studied the distribution of $P(\text{SG})_{\text{PCA}}$ among the components of the calibration sample, we found that only true SGs present values higher than $P(\text{SG})_{\text{PCA}} = 0.75$ (see Section 3.1.2). Thus, we were able to obtain a group of SGs a priori free from any non-SG (the “reliable SGs” set). In addition, it is possible to define an interval of probabilities between $P(\text{SG})_{\text{PCA}} = 0.75$ and a lower limit, that increases the selection of SGs, while keeping the contamination very low (the “probable SGs” set). The optimal lower limits for the Galactic samples were selected through the diagram shown

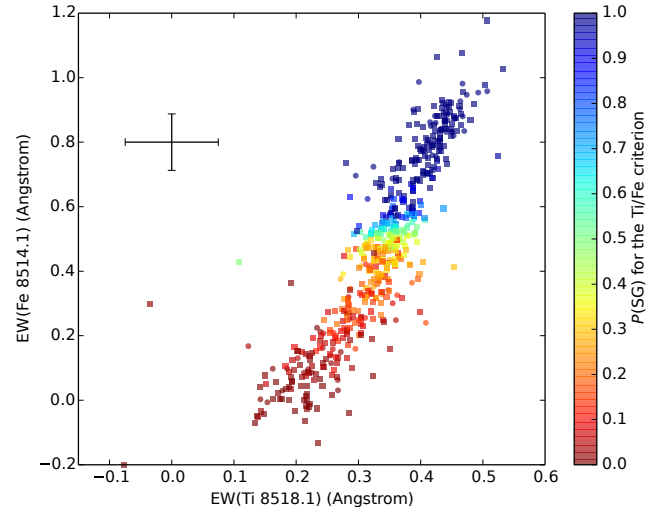


Figure 10. EWs of the FeI 8514 Å and TiI 8518 Å lines. The shapes indicate epoch: 2011 circles, 2012 squares. The black cross indicates the median uncertainties. The colour indicates $P(\text{SG})_{\text{Ti/Fe}}$. Comparison to Fig. 3 highlights the lack of stars with G and K spectral types.

Table 1. Number of targets tagged as “reliable SGs” or “probable SGs” (see 4.1) through the analysis of $P(\text{SG})_{\text{PCA}}$. The luminosity class was assigned through the manual classification. We also show the fraction that these groups represent with respect to the number of total targets in the sample (594). The 2-sigma uncertainties for the given fractions are equal to $1/\sqrt{n}$, where n is the total number of targets. Thus, the uncertainty of both fractions is equal to ± 0.04 .

Number			Fraction		
Reliable SGs	Probable SGs	Total	Reliable SGs	Probable SGs	Total
116	75	191	0.20	0.13	0.33

in Fig. 8, by the estimation of the inflexion point in the corresponding curve. For the Perseus sample we estimated it at $P(\text{SG})_{\text{PCA}} \sim 0.55$. The number of SGs found by these cuts is indicated in Table 1.

Classical methods are based on a linear boundary in a two-dimensional space. In consequence, when curves of $P(\text{SG})$ are plotted for them (see Section 3.1.2), there is no hint of a threshold value for “reliable SGs” as in the case of $P(\text{SG})_{\text{PCA}}$. Thus, the only reasonable minimum value, given the two-dimensional nature of the boundary, is $P(\text{SG}) = 0.5$. The number of targets identified as SGs are given in Table 2.

The targets tagged as SGs through $P(\text{SG})_{\text{PCA}}$ represent a significant fraction (almost one third) of the Perseus sample. Moreover, most of them ($\sim 66\%$) are tagged as “reliable SGs”; we can thus consider this group in good confidence free of any interloper. The number of SGs found through the PCA method is, however, significantly lower than the numbers found through the CaT and Ti/Fe criteria. We must be cautious with the results obtained using these methods, as their contaminations were higher (0.17 ± 0.13 for Ti/Fe and 0.20 ± 0.13 for CaT) than for the PCA (0.08 ± 0.13)

Table 2. Number of SGs found by different methods, and the fraction that they represent with respect to the total number of targets observed (594). For the classical criteria, we used a threshold of $P(\text{SG}) = 0.5$; for the PCA method, we adopted a threshold of $P(\text{SG}) = 0.55$ (see Sect. 3.2). The 2-sigma uncertainties of the fractions are equal to $1/\sqrt{n}$, where n is the total number of targets.

Criterion	Number of SGs	Fraction
CaT	304	0.51 ± 0.04
Ti/Fe	238	0.40 ± 0.04
PCA	193	0.32 ± 0.04

among MW stars in the calibration sample (see Paper III). The difference in the expected contamination is not enough to explain the number of stars tagged as SG, but it seems clear that the higher the contamination is for a method, the larger number of stars it identifies as SGs. Moreover, we have to take into account that the Galactic set from the calibration sample is limited in two ways. Firstly, the subsample was relatively small, which causes high uncertainties in our fractions (± 0.13). Secondly, this sample is not comparable to any observed sample, because it was intentionally created by assembling a similar number of well-known SGs and non-SGs. Thus, it will not be at all representative in terms of the number of non-SG stars that one may expect to find as interlopers when using photometric criteria to select SG candidates in the Galactic Plane. In view of these limitations, to study the efficiency and contamination of our methods in the Perseus sample, we resort to a direct calculation, in the next Section.

4.2 Efficiency of the photometric selection

The most important source of contaminants in the photometric selection comes from the magnitude/distance degeneracy. In this case, we are interested in structures relatively close to Earth, and in stars that are intrinsically bright, so we can enforce strict limits in apparent magnitude that will filter out most of the intrinsically dimmer populations along the line of sight. The overall efficiency of the selection criteria outlined in Sect. 2.1 is 47%. This includes the 43 MK standards mentioned in Section 2.2, as these were not included a posteriori but picked up by the selection algorithm.

As can be seen in Fig. 11, the efficiency decays with magnitude: at $m_{K_S} \sim 4.5$ most of the observed stars turn out to be interlopers. This agrees roughly with Paper I, as at the low end of the brightness distribution of SGs the selected sample is dominated by bright giants. Similarly, while the fraction of SGs is more or less homogeneous with colour, the red end of the distribution (stars with $(J - K_S) \geq 1.7$) is mostly composed of bright carbon stars. These results for a MW sample confirm those obtained in the MCs, in Paper I, and will also be useful for future photometric selections. However, we must caution that such a red cut-off can only be used to discriminate carbon stars in fields of low (such as the MCs) or moderate (like the present sample) extinction. For the high extinctions ($A_V \gtrsim 5$ mag) found in many lines of sight towards the inner Milky Way, M-type

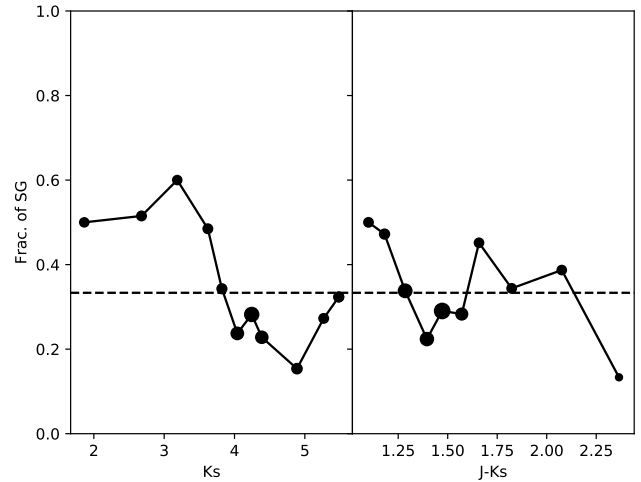


Figure 11. Fraction of SGs found in the target sample as a function of apparent K_S magnitude and colour. The dashed line marks the total average fraction, 47%. Of these detected SGs, $\sim 5\%$ were already known.

stars would be shifted to very high values of $(J - K_S)$ and other discriminants must be found.

4.3 Efficiency and contamination in the PCA method

4.3.1 Efficiency

To estimate directly the efficiency of our survey in the Perseus arm, we used the manual classification previously performed. We have to note that this classification is not *a priori* more reliable than our automatised methods. Manual classification was done before we developed the automated process detailed in Paper III. For the manual classification we used classical criteria, such as the EW of the Calcium Triplet, the ratio between nearby Ti and Fe lines (Fe I 8514 Å and Ti I 8518 Å among others) and the EW of the blend at 8468 Å. In Paper III, we demonstrated that the criteria based on these features have an efficiency slightly worse (at best) than our automated method. The manual classification can be somewhat better than these methods at identifying SGs, as it is a global process (like our PCA method), not based on any single spectral feature. Thus, the efficiency found in this work is useful to estimate the average quality of the classification methods under study with respect to a manual classification done following the classical criteria for the CaT range.

In the first place, we calculated the efficiency for each method (see Table 3). The efficiency in this case is the fraction of all SGs found through the manual classification, which were also tagged as such by a given automated criterion. The PCA method has the lowest global efficiency. It is similar to the value for the Ti/Fe criterion, but significantly lower than the efficiency of the CaT criterion. Nevertheless, when the LC of the targets is taken into account, the results can be seen in a very different light.

The calibration sample (see Paper III for details) is

Table 3. Number of targets from the Perseus sample tagged as SGs through the manual classification that were also identified as such by the different methods considered. Note that we found 241 SGs through the manual classification. Among them, 90 were classified as Ia or Iab, 85 as Ib, and 66 as Ib–II. Thus, the efficiencies, and their uncertainties (that are equal to $1/\sqrt{n}$) are calculated with respect to these values, and modified by the definition of efficiency (an efficiency > 1 is not possible).

Method	Number of SGs found				All	Efficiency		
	All	Ia to Iab	Ib	Ib–II		Ia to Iab	Ib	Ib–II
PCA	182	86	83	13	0.76 ± 0.06	$0.96^{+0.04}_{-0.11}$	$0.98^{+0.02}_{-0.11}$	0.20 ± 0.12
CaT	204	86	81	37	0.85 ± 0.06	$0.96^{+0.04}_{-0.11}$	$0.95^{+0.02}_{-0.11}$	0.56 ± 0.12
Ti/Fe	194	83	80	31	0.80 ± 0.06	$0.92^{+0.08}_{-0.11}$	$0.94^{+0.06}_{-0.11}$	0.47 ± 0.12

dominated by high- and mid-luminosity SGs (Ia and Iab), with only a small fraction of Ib or less luminous SGs (LC Ib–II). In consequence, our PCA method is optimized to find Ia and Iab SGs. In view of this, in the Perseus sample we considered the efficiency for different LCs separately. The efficiencies of the PCA and CaT criteria for high-luminosity SGs are the same, 0.96 ± 0.11 , and comparable to those found for the calibration sample. The efficiencies for low luminosity SGs (Ib) are also similar in both methods, and compatible with the results obtained for Ia and Iab stars. However, for the Ib–II stars the efficiencies are significantly different depending on the criterion used. The higher efficiency of the CaT method in the Ib–II group stems from the fact that this criterion is much less strict than the PCA one, but at the price of being more susceptible to contamination of red giants (see the following subsection). As the Ib–II subclass is the boundary between SGs (LC I) and bright giants (LC II), the morphology of the objects with this tag is intermediate. Moreover, there are AGB stars, which are not high-mass stars, whose spectra are pretty similar to those of a low luminosity SGs (Ib). The perfect example of this is α Her. This star is the high-luminosity MK standard with the latest spectral type available (M5 Ib–II; Keenan & McNeil 1989). However, Moravveji et al. (2013) show that this star is not a high-mass star ($M_* \gtrsim 10 M_\odot$), but an AGB star with a mass around $3 M_\odot$, even though its spectral morphology is very close to that of a SG. In view of this, through the manual classification we probably identified as SGs stars that are not really SGs, but pretty similar to them morphologically. The PCA criterion, instead, is more restrictive, and only selects as SGs those objects similar enough to the luminous (high-mass) SGs (those having LC Ia and Iab) used to calibrate it.

Our methods, and especially the PCA method, are very efficient for mid- to high-luminosity SGs (Iab to Ia), and also for lower luminosity supergiants (Ib). However, there is also a small number of stars (6) manually classified between Ia and Ib that were not identified as SGs by the PCA. All these 6 stars have mid- to late-M types. All but one of them are M5 or later, with most of them (four) having very late SpTs (M7 or M7.5). In fact, these stars are the majority of the RSGs with SpTs M5 or later in the whole Perseus sample, as there are only two other M5 Ib stars (which were correctly identified by the PCA method). The only star earlier than M5 (it was classified as M3) which was not identified as a SG is S Per, an extreme RSG (ERSG). The reason why this object was not correctly identified is clear: its lines are weakened by veiling, an effect that may appear in ERSG stars

which has been reported before for S Per (Humphreys 1974). For more details about ERSGs and veiling, see Section 4.4 from Paper III and references therein.

Just like the PCA method, the CaT and the Ti/Fe criteria fail for mid- to late-M SGs. They failed to identify the same true supergiants that were not found by the PCA. In addition, they also failed for a group of Ia to Ib stars with slightly earlier SpTs (M3 and M4). The obvious conclusion is that all methods fail almost completely in the identification of mid- to late-M RSGs. However, the PCA method provides significantly better results for mid-M SGs (up to M5) than the other criteria. This, in turn, cannot be considered a major drawback, as the number of mid- to late-M RSGs is very small, with only a handful of supergiants presenting spectral types later than M5 (and most of them presenting spectral variability).

4.3.2 Contamination

The three identification methods studied above have similar efficiencies for mid- to high-luminosity subsamples. The advantage of the PCA method over the other two is to provide significant lower contaminations, at least for the calibration sample. Therefore, we estimated the contamination obtained through each method for the Perseus sample. The contamination in this case is the fraction of the stars selected as SGs by a given automated criterion that were not identified as real SGs through the manual classification. The results are shown in Table 4.

The method with the lowest contamination is by far PCA. All the non-SGs wrongly selected by the $P(\text{SG})$ have LC II in the manual classification, and therefore their spectra are very similar morphologically to those of low-luminosity RSGs. Indeed, we cannot dismiss a priori the possibility that they may be low-luminosity SGs wrongly identified in the manual classification. The Ti/Fe criterion has a significantly higher contamination, but the CaT criterion works significantly worse than the other two in this respect. This is not completely unexpected, as the strength of the CaT lines is not only a function of luminosity, but also effective temperature and metallicity (Diaz et al. 1989).

The contamination found in the Perseus sample through the PCA method (0.06 ± 0.07) is compatible with those obtained for the calibration sample (0.03 ± 0.04) and its MW subset (0.08 ± 0.13) in Paper III. In the case of the CaT and Ti/Fe methods, their contaminations when applied to the MW subset of the calibration sample are 0.17 ± 0.13 for the Ti/Fe criterion and 0.20 ± 0.13 for the CaT criterion, which

Table 4. Contaminations obtained through different methods for the Perseus sample. As the contamination is the fraction of targets tagged as SGs that actually are not SGs, its 2-sigma uncertainty is equal to $1/\sqrt{n}$, where n is the number of objects identified as SGs.

Method	Number of targets tagged as SGs	Number of non-SGs wrongly identified	Contamination
PCA	193	11	0.06 ± 0.07
CaT	304	100	0.33 ± 0.06
Ti/Fe	238	43	0.18 ± 0.07

are again compatible with those obtained in this work for these methods (see Table 4). Therefore the results for the Perseus sample corroborate the conclusions that we reached based on the subsample of MW stars in the calibration sample in Paper III, this time for a significantly larger sample.

4.4 The population of cool supergiants in Perseus

As explained in Section 3.2, with the values proposed for the $P(\text{SG})_{\text{PCA}}$ we identified 191 targets as SGs in Perseus (86 of them having LC Ia or Iab according to the manual classification), while our manual identification found 258 (96 of them having LC Ia or Iab), including all the 191 PCA SGs. The difference between both sets is mainly due to Ib–II stars, which, as discussed above, may in fact not be true SGs, but bright giants. The rest of the difference is due to the late-M stars, which are not correctly selected by any of the automated criteria studied, even though their SG nature is very likely. Thus, for the present analysis we decided to adopt the PCA selection, but also include the five SGs (Ia to Ib) with late subtypes (M5 to M7) that were identified through manual classification, as well as S Per, which is a well-known ERSGs (see Sect. 4.3.1).

The supergiant content of the Perseus arm was studied by Humphreys (1970, 1978), who found more than 60 CSGs in this region. Later, Levesque et al. (2005) studied the RSG population of the Galaxy, adding a handful of new stars to the list of known RSGs in the Perseus arm. We also took into account a small number of CSG standards from Keenan & McNeil (1989) located in the Perseus arm. Using these works and crossing their lists, we obtained a list of 77 previously known CSGs in the Perseus arm. Among the 197 CSGs we found, there are only six that were included in this list. Thus, our work increases the number of CSGs known in Perseus in 191 stars, more than trebling the size of previous compilations (from 77 to 268 CSGs).

This large number of CSGs allows us to study statistically the population of CSGs in the Perseus arm with unprecedented significance. Indeed, this sample permits a direct comparison of the CSG population in the Perseus arm and those in the MCs studied in Paper II. For this analysis, we used the SpT and LC given through the manual classification for the CSGs in our Perseus sample, and the classification given in the literature for the rest of the Perseus SGs that had gone to the calibration sample. Unfortunately, the distances to many of these stars still have significant uncertainties, which do not allow us to compare absolute magnitudes. However, in the near future *Gaia* will provide reliable and homogeneous distances for almost all of them. We will then use these distances together with the radial velocities

obtained from our spectra (which can be compared to the *Gaia*/RVS radial velocities to detect binarity) to study in detail the spatial and luminosity distributions for the CSG population in the Perseus arm. In the present work we only analyse the SpT and LC distributions.

When previous works have analysed a given population of RSGs, they have typically found their SpTs to be distributed around a central subtype with maximum frequency. In all populations, the frequency of the subtypes is lower the farther away from the central value the subtype is. The central subtype is related to the typical metallicity of the population, with later types for higher metallicities (Humphreys 1979; Elias et al. 1985). This effect has been confirmed by recent works for different low-metallicity environments (Levesque & Massey 2012). In Paper II we confirmed this effect for very large samples in both MCs.

The SpT distribution of the Perseus CSGs found in the present work (the PCA selection plus the six late RSGs visually identified) is shown in Fig. 12. The median SpT of this sample is M1. We also studied the global population (268 CSGs), which includes all the previously known RSGs from the Perseus arm together with all our newly-found CSGs. Its histogram is shown in Fig. 13a. Addition of the set of previously known RSGs not included in our own sample (see Fig. 13a) shifts very slightly the median type to M1.5. Both median types are slightly earlier than values typically given for the MW according in the literature (M2; Elias et al. 1985; Levesque 2013). However, the difference is not large enough to be truly significant, given the typical uncertainty of one subtype in our manual classifications. We can thus consider our results consistent with the value found in the literature. Despite this, we note that our sample is intrinsically different from any previous sample of Galactic RSGs. With the possible exception of a few background RSGs (which could be present given our magnitude cut, but should be very rare, because of the steeply falling density of young stars towards the outer Milky Way), our sample is volume-limited; it represents the total RSG population for a section of a Galactic arm. Previous works are mostly magnitude-limited and therefore tend to include an over-representation of later-type M supergiants, as these objects tend to be intrinsically brighter (see Paper II and references therein).

The SpT distribution shown presents a clear asymmetry due to the presence of a local maximum at early-K types. This local maximum was not detected by Elias et al. (1985), but is present in Levesque (2013), in their figure 1. The SGs considered in Elias et al. (1985) were mainly of luminosity classes Ia and Iab, while most of the early-K SGs used in Levesque (2013) are of Ib class. This is also the case in our sample; most early-K (K0–K3) supergiants present low

luminosity classes (Ib or less, see Fig. 13b). Studies of similar stars in open clusters (e.g. [Negueruela & Marco 2012](#); [Alonso-Santiago et al. 2017](#)), show that these low-luminosity supergiants with early-K types are in general intermediate-mass stars (of $6-8 M_{\odot}$), with typical ages (~ 50 Ma) much older than luminous RSGs (typically between 10 and 25 Ma). Therefore, despite their morphological classification as SGs, these stars should not be considered as true supergiants, because they are not quite high-mass stars. These stars are not very numerous in our sample (we have 19 stars with early-K types and LC Ib or less luminous) nor in the total population (23 stars). Therefore, our median types do not change if we do not consider these stars as part of the CSG population. It is worthwhile stressing that there are very few K-type true supergiants in the Milky Way, to the point that the original list of MK standards contains only one such object (the K3 Iab standard α^1 Cma, later moved to K2.5 Iab; [Morgan & Keenan 1973](#)), as opposed to five K Ib stars, representative of the lower-mass population discussed above (see [Johnson & Morgan 1953](#)). This absence of K-type SGs represents the main difference between the present catalogue and those from the MCs, as illustrated by Fig. 13b.

In [Paper II](#), we found that RSGs in the MCs present a relation between SpTs and LCs, with later typical types for Ia than for Iab stars. As a consequence, we found an earlier typical SpT for each MC than in previous works by a few subtypes. This difference was caused by the inclusion in our survey of a large number of Iab CSGs, while previous studies studied were centred on the brightest RSGs, mostly Ia (see sect. 4.2 of [Paper II](#)). In contrast, when we analyse the different LC subsamples in Perseus, we do not find any significant difference between Ia and Iab stars, as both groups have the same median SpT: M1 (see Fig. 13b). When we consider the global population, Iab supergiants have a median type of M1.5, but a difference of half a subtype cannot be considered significant. These results contrast strongly with the trends found in the MCs. It is unclear, though, if we can derive any reliable conclusions from this difference, because the number of Ia stars in the Perseus sample is too low compared to the number of Iab stars: seven Ia against 83 Iab in our sample; 19 Ia against 116 Iab in the global population.

There are a number of factors to consider before attempting any interpretation. Firstly, there are four early K-type Ia SGs pushing the median type to early types. As mentioned, these spectral types are rare in the MW, and many of these objects present unusual characteristics, such as evidence for binary interaction or heavy mass loss. Due to the small size of the Ia sample, these rare objects may have a disproportionate impact on the average type. Moreover, we may be biasing our sample because of a classification issue: there are no MK SG standards for spectral types later than M4 (except for α Her, mentioned above, which is not a true SG). At these spectral types, luminosity indicators are strongly affected by the molecular bands, specially TiO bands. In fact, for types later than M3, many luminosity indicators (e.g. the Ca Triplet) do not separate RSGs from red giants ([Dorda et al. 2013](#), [Paper II](#), and [Paper III](#)). Our sample contains a number of RSGs with mid to late types, which were given a generic I classification, as it was not possible to give a more accurate luminosity subclass (see discussion in [Negueruela et al. 2012](#)). For calculation purposes, these

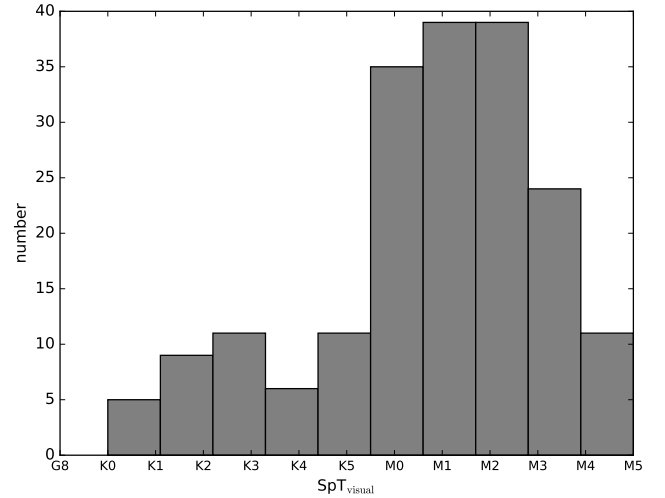


Figure 12. Distribution of SpTs for the targets identified as SGs using the PCA method.

objects have been assigned to the intermediate luminosity Iab. This could be incorrect, as the few late-M RSGs found in open clusters tend to have much higher luminosities than earlier RSGs in the same clusters ([Negueruela et al. 2013](#); [Marco & Negueruela 2013](#)).

Within our sample, we have an interesting example of the situation explained above in the cluster NGC 7419. This rich cluster contains five RSG members; four of them have M0 to M2 Iab types, while the last one, MY Cep, is M7.5 I ([Marco & Negueruela 2013](#)). As can be seen in fig. 13 of [Marco & Negueruela \(2013\)](#), MY Cep is about one and a half magnitude more luminous than the other 4 RSGs. As MY Cep was the only comparison star available for the manual classification of the late RSGs in our sample, it is reasonable to expect that the three stars classified as M7 I could also be high luminosity RSGs, as MY Cep is. Four other Ia stars present types M3 to M4. One of them is S Per, a known spectral variable that can present types as late as M7, according to [Fawley \(1977\)](#). In view of this, it is highly likely that we are underestimating the number of late-M Ia RSGs. Even though these are also rare objects, given the small size of the Ia sample, they could move the median to later types. In this context, it is important to note that the MC populations studied in [Paper II](#) include very few mid- or late-M supergiants. Most MC Ia RSGs were M3 or earlier, allowing their LC classification without the complications that affect luminosity indicators at later types. In addition, the distance to the RSGs in the MCs is well known, allowing a direct knowledge of the actual luminosity. In the Perseus sample, we have to resort only to morphological characteristics in most cases, at least until accurate distances are provided by *Gaia*.

The low number of Ia SGs may be meaningful in itself. On one side, magnitude-limited samples will always have a bias towards intrinsically bright stars that is not present in the Perseus sample. On the other side, the sample of CSGs in the SMC presented in [Paper I](#), which may not be complete, but is at least representative, has a much higher fraction of Ia supergiants with respect to the Iab cohort. As discussed in [Paper II](#), there may be two different pathways leading

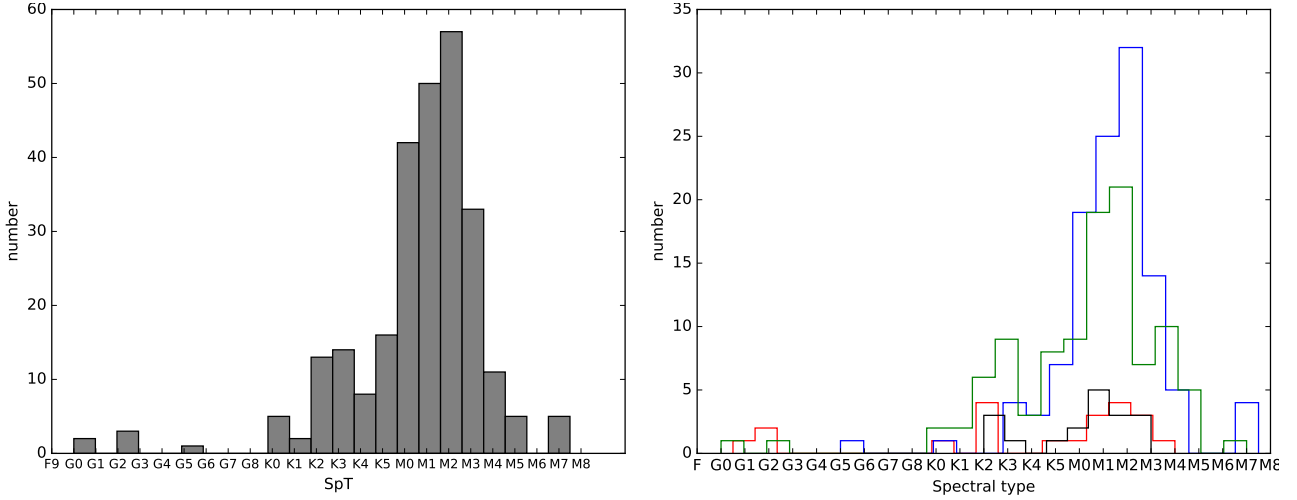


Figure 13. Left (13a): Distribution of SpTs for Perseus CSGs (our sample plus previous identifications). Right (13b): The same sample as in left panel, but split by luminosity class, with red for Ia, blue for Iab, green for Ib, and black for Ib–II.

to high-luminosity CSGs. Since stellar evolutionary models (Ekström et al. 2012; Georgy et al. 2013; Brott et al. 2011) indicate that evolution from the hot to the cool side of the HR diagram happens at approximately constant luminosity, the brightest CSGs should be descended from more massive stars (with masses $\sim 25M_{\odot}$ and up to $\sim 40M_{\odot}$). On the other hand, observations of open clusters (Negueruela et al. 2013; Beasor & Davies 2016) suggest that less massive stars (with masses between 10 and $\sim 20M_{\odot}$) could evolve from typical Iab CSGs towards higher luminosities and cooler temperatures at some point in their lives. This idea is suggested by the presence in massive clusters of some RSGs with significantly later SpTs and much higher luminosities than most of the other RSGs in the same cluster (as in the example of NGC 7419 mentioned above).

The low fraction of Ia CSGs in the Perseus arms may shed some light on these issues. Although there are some very young star clusters and associations (mainly Cep OB1 and Cas OB6) in the area surveyed, most of the clusters and OB associations are not young enough to still have any RSGs with high masses ($\gtrsim 20M_{\odot}$). The most massive clusters included in the sample region have ages around 15 Ma, with main-sequence turn-offs at B1 V. This is the case of NGC 7419 (Marco & Negueruela 2013) or the double Perseus cluster, the core of the Perseus OB1 association (Slesnick et al. 2002), while the clusters in Cas OB8 are even older. For an age ~ 15 Ma, according to Geneva evolutionary models (Ekström et al. 2012), RSGs should be descended from stars with an initial mass $\sim 15M_{\odot}$ and not be much more luminous than $M_{\text{bol}} \sim -7$. As can be seen in fig. 16 of Paper II, most Ia RSGs are more luminous than this value. Therefore, the scarcity of Ia RSGs in Perseus can be interpreted as a straight consequence of the lack of high-mass RSGs, which supports the idea that Ia CSGs come mainly from stars with initial masses between 20 and $40M_{\odot}$. However, there still is a significant fraction (0.07 ± 0.06) of Ia stars, which are not directly related to any very young cluster. For example, following with the example of Per OB1, this association contains the well known ERSR S Per (Humphreys 1978), which has been observed to vary from M4 to M7Ia. This

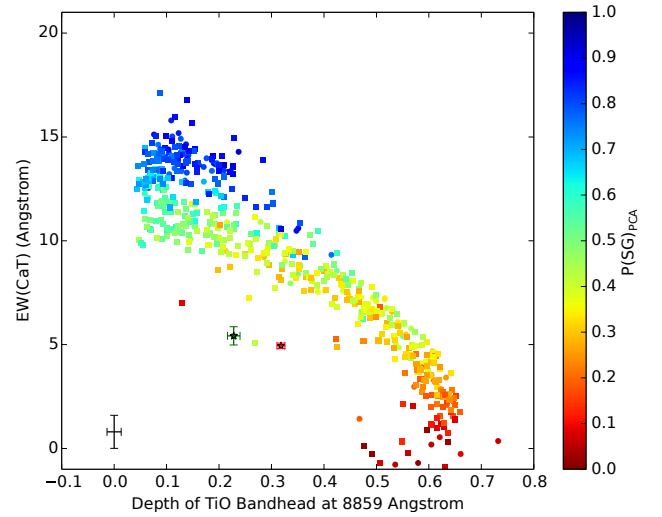


Figure 14. Depth of the TiO bandhead at 8859 \AA with respect to the sum of the EWs of the CaT lines, for the Perseus sample. The colour indicates $P(\text{SG})_{\text{PCA}}$, and the shapes indicate epoch (2011 circles, 2012 squares), except for the two stars, which are reference ERSRs. The green star is the S Per and the red star is UY Sct. Both ERSRs are represented with their own error bars. The black cross indicates the median uncertainties of the sample. The scale used in this Figure is the same as for Fig. 14a from Paper III, which show the same diagram for the calibration sample, to ease the comparison.

suggests that indeed some intermediate mass RSGs may increase their luminosity up to LC Ia from lower luminosities. Their low number in the sample agrees with small fraction of very luminous RSGs found in massive open clusters.

4.5 Candidates to extreme red supergiants

In Paper III we proposed the use of two diagrams to detect RSGs affected by veiling, a characteristic effect that ERSRs present at some points in their spectral variation (for details

about veiling see [Humphreys 1974](#), and Section 4.4 in [Paper III](#)). In Fig. 14 we include the location of the two veiled ERSs, UY Sct and S Per (which indeed is one of the stars in the Perseus sample), that were available to us. They indicate the typical region where veiled ERSs seem to lie. For the Perseus sample we found only one star close to them, outside the main band of giant and supergiant stars. This object, PER433, was rejected as a SG by the $P(\text{SG})_{\text{PCA}}$ (and also by the other methods), but given the effect of veiling on atomic lines, this rejection cannot be considered conclusive. In the bibliography this object, known as V627 Cas, has been identified as some kind of symbiotic star ([Kolotilov et al. 1996](#)). We checked its spectrum and found that it shows the OI line at 8448 Å in emission, which is usual in Be stars, but not expected in ERSs, since it requires higher temperatures. It also has its CaT lines in emission, partially filling them, which explains why this star shows EW(CaT) much smaller than expected for a giant star. Therefore, we can conclude that this star is not an ERS.

5 CONCLUSIONS AND FUTURE WORK

In [Paper III](#) we proposed a method for using PCA in the identification of CSGs. In the present work we have developed it further, obtaining a way to estimate the probability that a given spectrum is a CSG, instead of just giving a binary result (“SG” or “non-SG”). We have then applied this method to a large sample of galactic stars selected to be part of the Perseus arm. We also compared the results obtained through the method using PCA with two other classical criteria studied in [Paper III](#) (those based on the CaT and Ti/Fe criteria). Summarising, from the analysis presented in this work we can conclude:

(i) We find that the efficiencies of all three automated methods are similarly high ($> 90\%$) for objects which were visually classified as certain CSGs (Ia to Ib), and compatible with those obtained for the calibration sample in [Paper III](#). The results are much worse in the case of those targets visually classified as Ib–II for the three methods, and especially for the PCA one. However, this group of LC Ib–II objects is probably formed mostly by non-SGs and the automated methods could be simply pointing this out. Finally, we find that the efficiency is almost zero for stars visually identified as SGs having subtypes later than M5, independently of the method used.

(ii) Although the efficiencies are similarly good in the three cases, the contaminations are very different for each method, when manual classification is used as a reference. As in the case of the MCs, the PCA method provides the cleanest sample of SGs, with a contamination fraction as low as 0.06 ± 0.07 , against 0.33 ± 0.06 and 0.18 ± 0.07 for the CaT and Ti/Fe criteria. The contamination found for the PCA method is compatible with that obtained for the calibration sample of [Paper III](#). However, the other two methods result in values significantly higher, probably because the Perseus sample has a larger fraction of bright M giants than our MC samples, because in this case we are observing through the Galactic plane.

(iii) Using the PCA method, we identified 191 targets as CSGs, plus 6 RSGs with late SpTs which were identified

through the manual classification. These 197 CSGs are a significant fraction of the total sample (0.33 ± 0.04), demonstrating that the photometric selection criteria used have a very high efficiency at moderate reddenings. This sample represents the largest catalogue of CSGs in the MW observed homogeneously, increasing the census of catalogued CSGs in the Perseus arm dramatically: to the 77 CSGs contained in previous lists, this catalogue adds 191 more objects. The list of stars observed, with their corresponding probabilities of being a SG through different methods is given in Tables A1.

The final catalogue, with almost 200 CSGs, is the largest coherent sample of CSGs observed to date in the Galaxy. In the future, we will use this sample to study both the CSG population and its relation to structure of the Perseus arm. We will use the radial velocities that we can obtain from our spectra, along with *Gaia* distances (which will be available for these stars by mid 2018), to study the spatial distribution of the CSGs in the Perseus arm and their relation with nearby clusters and OB associations. In addition, we will also analyse the physical properties of these stars, deriving them from their spectra by using the method that we are developing (Tabernero et al. in prep.). Finally, it is our intention to extend the study of CSG populations toward the inner Galaxy, where we should find higher metallicities, but will also have to fight much higher extinction and stellar densities

ACKNOWLEDGEMENTS

We thank the referee, Prof. Roberta Humphreys, for the swiftness of her response. The INT is operated on the island of La Palma by the Isaac Newton Group in the Spanish Observatorio del Roque de Los Muchachos of the Instituto de Astrofísica de Canarias. This research is partially supported by the Spanish Government Ministerio de Economía y Competitividad (MINECO/FEDER) under grant AYA2015-68012-C2-2-P. This research has made use of the Simbad, Vizier and Aladin services developed at the Centre de Données Astronomiques de Strasbourg, France. This research has made use of the WEBDA database, operated at the Department of Theoretical Physics and Astrophysics of the Masaryk University. It also makes use of data products from the Two Micron All Sky Survey, which is a joint project of the University of Massachusetts and the Infrared Processing and Analysis Center/California Institute of Technology, funded by the National Aeronautics and Space Administration and the National Science Foundation. This research has made use of the SIMBAD database, operated at CDS, Strasbourg, France

REFERENCES

- Alonso-Santiago J., Negueruela I., Marco A., Tabernero H. M., González-Fernández C., Castro N., 2017, [MNRAS](#), **469**, 1330
- Beasor E. R., Davies B., 2016, [MNRAS](#), **463**, 1269
- Brott I., et al., 2011, [A&A](#), **530**, A115
- Choi Y. K., Hachisuka K., Reid M. J., Xu Y., Brunthaler A., Menten K. M., Dame T. M., 2014, [ApJ](#), **790**, 99
- Davies B., et al., 2013, [ApJ](#), **767**, 3
- Diaz A. I., Terlevich E., Terlevich R., 1989, [MNRAS](#), **239**, 325

- Dorda R., Negueruela I., González-Fernández C., 2013, in Kervella P., Le Bertre T., Perrin G., eds, EAS Publications Series Vol. 60, EAS Publications Series. pp 299–304, [doi:10.1051/eas/1360035](#)
- Dorda R., Negueruela I., González-Fernández C., Tabernero H. M., 2016a, [A&A](#), **592**, [A16](#)
- Dorda R., González-Fernández C., Negueruela I., 2016b, [A&A](#), **595**, [A105](#)
- Ekström S., et al., 2012, [A&A](#), **537**, [A146](#)
- Ekström S., Georgy C., Meynet G., Groh J., Granada A., 2013, in Kervella P., Le Bertre T., Perrin G., eds, EAS Publications Series Vol. 60, EAS Publications Series. pp 31–41 ([arXiv:1303.1629](#)), [doi:10.1051/eas/1360003](#)
- Elias J. H., Frogel J. A., Humphreys R. M., 1985, [ApJS](#), **57**, [91](#)
- Fawley W. M., 1977, [ApJ](#), **218**, [181](#)
- Georgy C., et al., 2013, [A&A](#), **558**, [A103](#)
- González-Fernández C., Dorda R., Negueruela I., Marco A., 2015, [A&A](#), **578**, [A3](#)
- Humphreys R. M., 1970, [ApJ](#), **160**, [1149](#)
- Humphreys R. M., 1974, [ApJ](#), **188**, [75](#)
- Humphreys R. M., 1978, [ApJS](#), **38**, [309](#)
- Humphreys R. M., 1979, [ApJ](#), **231**, [384](#)
- Humphreys R. M., Davidson K., 1979, [ApJ](#), **232**, [409](#)
- Johnson H. L., Morgan W. W., 1953, [ApJ](#), **117**, [313](#)
- Keenan P. C., McNeil R. C., 1989, [ApJS](#), **71**, [245](#)
- Kolotilov E. A., Munari U., Yudin B. F., Tatarnikov A. M., 1996, *Astronomy Reports*, **40**, [812](#)
- Levesque E. M., 2013, in Kervella P., Le Bertre T., Perrin G., eds, EAS Publications Series Vol. 60, EAS Publications Series. pp 269–277 ([arXiv:1302.0822](#)), [doi:10.1051/eas/1360031](#)
- Levesque E. M., Massey P., 2012, [AJ](#), **144**, [2](#)
- Levesque E. M., Massey P., Olsen K. A. G., Plez B., Josselin E., Maeder A., Meynet G., 2005, [ApJ](#), **628**, [973](#)
- Levesque E. M., Massey P., Olsen K. A. G., Plez B., 2007, [ApJ](#), **667**, [202](#)
- Marco A., Negueruela I., 2013, [A&A](#), **552**, [A92](#)
- Monet D. G., et al., 2003, [AJ](#), **125**, [984](#)
- Moravveji E., Guinan E. F., Khosroshahi H., Wasatonic R., 2013, [AJ](#), **146**, [148](#)
- Morgan W. W., Keenan P. C., 1973, [ARA&A](#), **11**, [29](#)
- Negueruela I., Marco A., 2012, [AJ](#), **143**, [46](#)
- Negueruela I., Marco A., González-Fernández C., Jiménez-Esteban F., Clark J. S., Garcia M., Solano E., 2012, [A&A](#), **547**, [A15](#)
- Negueruela I., González-Fernández C., Dorda R., Marco A., Clark J. S., 2013, in Kervella P., Le Bertre T., Perrin G., eds, EAS Publications Series Vol. 60, EAS Publications Series. pp 279–285 ([arXiv:1303.1837](#)), [doi:10.1051/eas/1360032](#)
- Slesnick C. L., Hillenbrand L. A., Massey P., 2002, [ApJ](#), **576**, [880](#)
- Zacharias N., et al., 2010, [AJ](#), **139**, [2184](#)

APPENDIX A: SAMPLE OBSERVED

Table A1: Small sample of the stars we observed in the Perseus arm. We include for each target the observation epoch, the manual classification done, the calculated probabilities of being a SG (obtained through the PCA method as well as the CaT or Ti/Fe criteria). For more details see Section 3.

ID	RA J2000	DEC J2000	l (deg)	b (deg)	Epoch	Visual Classification	P _{PCA}	P _{CaT}	P _{Ti/Fe}
PER001	0:00:10.00	+62:27:36.0	117.044	0.17579	2011	M6.0 II	0.429	0.035	0.251
PER002	0:00:18.00	+60:21:02.0	116.644	-1.89536	2011	M4.5 Ib – II	0.513	0.345	0.299
PER003	0:01:44.20	+62:11:23.8	117.171	-0.12456	2012	M3.0 II	0.595	0.998	0.5
PER004	0:01:46.90	+64:16:36.8	117.575	1.92282	2012	M6.0 II – III	0.364	0.0	0.073
PER005	0:02:20.00	+57:02:14.1	116.261	-5.19714	2012	M8.0 III	0.117	0.0	0.0
PER006	0:02:59.00	+61:22:05.0	117.160	-0.95948	2011	M3.0 Ib – II	0.39	0.998	0.636
PER007	0:04:10.80	+60:55:22.3	117.220	-1.42367	2012	C star	–	–	–
PER008	0:06:39.00	+58:02:18.0	117.015	-4.31797	2011	M5.0 Ib – II	0.357	0.157	0.277
PER009	0:08:58.40	+62:42:57.0	118.087	0.24419	2012	C star	–	–	–
PER010	0:09:26.30	+63:57:14.0	118.341	1.45716	2012	M2.0 Iab	0.879	1.0	1.0
PER011	0:10:49.60	+64:51:14.2	118.633	2.32174	2012	M6.5 II	0.374	0.009	0.14
PER012	0:12:21.60	+62:53:33.6	118.497	0.35787	2012	K0.0 Iab	0.64	1.0	1.0
PER013	0:13:23.20	+63:27:31.2	118.696	0.90028	2012	C star	–	–	–
PER014	0:14:57.50	+66:37:30.3	119.318	4.00967	2012	M1.0 II	0.498	0.998	0.641
PER015	0:15:01.00	+66:06:50.2	119.251	3.50283	2012	K3.0 Ib – II	0.501	1.0	0.939
PER016	0:16:42.30	+67:33:02.8	119.615	4.90300	2012	M4.0 II	0.408	0.353	0.443
PER017	0:16:54.90	+57:31:51.1	118.293	-5.02962	2012	M7.5 II	0.332	0.0	0.065
PER018	0:18:23.00	+61:52:28.0	119.047	-0.74769	2011	M6.0 II	0.278	0.0	0.073
PER019	0:18:26.40	+60:54:08.9	118.929	-1.71255	2012	M1.0 Iab	0.811	1.0	1.0
PER020	0:19:03.00	+57:43:42.2	118.603	-4.87090	2012	M6.0 III	0.329	0.0	0.048
PER021	0:19:04.10	+66:22:13.1	119.691	3.70249	2012	C star	–	–	–
PER022	0:20:43.50	+61:52:46.5	119.321	-0.77665	2012	M1.0 Iab	0.794	1.0	1.0
PER023	0:21:31.80	+61:31:13.5	119.374	-1.14453	2012	M3.0 Ib – II	0.445	0.837	0.358
PER024	0:22:26.80	+59:11:33.4	119.220	-3.47006	2012	C star	–	–	–
PER025	0:23:17.00	+62:21:39.0	119.673	-0.33264	2011	M6.5 III	0.215	0.0	0.012
PER026	0:26:18.00	+61:41:19.0	119.956	-1.03778	2011	M6.0 II	0.311	0.007	0.077
PER027	0:26:18.70	+61:32:03.1	119.942	-1.19160	2012	M1.5 II	0.543	1.0	0.755
PER028	0:27:11.00	+63:33:25.0	120.236	0.81225	2011	M6.0 Ib – II	0.444	0.001	0.049
PER029	0:27:29.00	+59:19:47.7	119.876	-3.39962	2012	M5.0 III	0.407	0.005	0.196
PER030	0:28:08.50	+60:29:29.5	120.065	-2.25047	2012	M6.0 Ib – II	0.262	0.0	0.047
PER031	0:28:40.00	+63:27:40.0	120.392	0.70174	2011	M2.0 Ib	0.786	1.0	1.0
PER032	0:29:48.50	+60:29:43.4	120.270	-2.26451	2012	K2.0 Ib	0.626	1.0	1.0
PER033	0:30:26.20	+67:00:06.2	120.877	4.21378	2012	M1.5 II	0.396	1.0	0.86
PER034	0:30:59.50	+61:26:19.0	120.490	-1.33615	2012	M0.0 Ib	0.611	1.0	0.962
PER035	0:31:25.40	+60:15:19.5	120.449	-2.51982	2012	M0.0 II	0.492	1.0	0.699
PER036	0:33:47.10	+58:15:37.3	120.605	-4.53160	2012	M5.0 III	0.387	0.067	0.251
PER037	0:34:31.00	+61:56:42.0	120.944	-0.86140	2011	M7.0 III	0.201	0.0	0.01
PER038	0:35:02.70	+61:19:02.1	120.966	-1.49189	2012	C star	–	–	–
PER039	0:35:26.00	+61:14:48.0	121.008	-1.56527	2011	M7.0 II	0.249	0.0	0.024
PER040	0:35:37.10	+67:55:33.0	121.441	5.09990	2012	K3.0 Iab	0.728	1.0	1.0
PER041	0:35:41.10	+64:09:07.9	121.216	1.33296	2012	C star	–	–	–
PER042	0:35:42.00	+63:07:47.0	121.155	0.31229	2011	M0.0 Ib	0.756	1.0	1.0
PER043	0:37:16.50	+58:46:24.2	121.093	-4.04777	2012	M5.0 III	0.313	0.066	0.158
PER044	0:38:28.00	+63:14:09.0	121.472	0.40086	2011	M2.0 Iab	0.811	1.0	1.0
PER045	0:38:42.40	+61:43:57.4	121.425	-1.10188	2012	M2.0 Ib – II	0.423	0.998	0.574
PER046	0:40:01.00	+62:19:41.0	121.606	-0.51429	2011	M0.5 Ib	0.815	1.0	1.0
PER047	0:40:24.80	+59:30:49.7	121.532	-3.32797	2012	M2.0 Ib	0.618	1.0	0.913
PER048	0:40:28.00	+64:17:33.0	121.742	1.44610	2011	M1.5 Ib	0.797	1.0	1.0
PER049	0:41:24.10	+59:24:41.4	121.653	-3.43533	2012	M0.0 Ib – II	0.53	1.0	0.803
PER050	0:43:51.00	+62:16:51.0	122.050	-0.57791	2011	M1.0 Iab	0.868	1.0	1.0
PER051	0:44:00.90	+58:56:05.5	121.972	-3.92305	2012	M6.0 II	0.443	0.0	0.081

Table A1: continued.

ID	RA J2000	DEC J2000	l (deg)	b (deg)	Epoch	Visual Classification	P _{PCA}	P _{CaT}	P _{Ti/Fe}
PER052	0:44:32.00	+62:07:15.0	122.125	-0.74009	2011	M0.0 Ib	0.706	1.0	1.0
PER053	0:45:51.50	+58:02:18.4	122.191	-4.82528	2012	M6.0 II	0.358	0.025	0.133
PER054	0:48:34.00	+62:04:23.0	122.596	-0.79682	2011	M5.0 Ib – II	0.368	0.086	0.213
PER055	0:49:11.00	+64:56:19.0	122.693	2.06791	2011	M3.0 Ib	0.827	1.0	1.0
PER056	0:49:17.60	+63:10:05.3	122.690	0.29740	2012	M4.5 II – III	0.498	0.407	0.246
PER057	0:50:25.00	+63:03:05.0	122.816	0.17987	2011	M4.5 Ib – II	0.471	0.065	0.162
PER058	0:50:38.40	+60:13:07.1	122.833	-2.65296	2012	S star	0.509	0.864	0.966
PER059	0:52:49.70	+57:24:23.7	123.120	-5.46466	2012	M5.0 III	0.297	0.113	0.196
PER060	0:53:38.00	+63:20:29.0	123.178	0.47069	2012	C star	–	–	–
PER061	0:54:53.80	+58:33:49.2	123.384	-4.30504	2012	C star	–	–	–
PER062	0:55:09.80	+57:16:34.1	123.438	-5.59195	2012	M1.0 Ib	0.667	1.0	1.0
PER063	0:57:31.70	+60:20:12.2	123.686	-2.52611	2012	M6.0 II – III	0.411	0.007	0.144
PER064	0:57:35.80	+61:28:08.1	123.667	-1.39403	2012	M7.0 III	0.245	0.0	0.0
PER065	0:58:02.00	+62:49:32.0	123.685	-0.03655	2011	M2.0 Iab	0.814	1.0	1.0
PER066	0:58:04.30	+67:41:51.8	123.563	4.83411	2012	M1.5 II	0.457	1.0	0.519
PER067	0:58:12.30	+59:34:24.0	123.790	-3.28714	2012	M1.0 Iab	0.8	1.0	1.0
PER068	1:00:26.00	+63:33:16.0	123.933	0.70019	2011	M3.0 II	0.526	0.998	0.89
PER069	1:01:58.40	+57:59:48.2	124.332	-4.84637	2012	M7.5 III	0.191	0.0	0.02
PER070	1:02:43.60	+61:51:43.0	124.263	-0.98063	2012	C star	–	–	–
PER071	1:02:44.00	+60:36:15.4	124.319	-2.23705	2012	M6.0 III	0.28	0.019	0.198
PER072	1:02:55.70	+60:58:23.9	124.326	-1.86733	2012	M0.5 Ib	0.7	1.0	1.0
PER073	1:03:15.00	+63:05:11.0	124.268	0.24529	2011	M5.0 Ib – II	0.389	0.204	0.337
PER074	1:03:33.60	+61:12:31.5	124.392	-1.62864	2012	M2.0 II	0.44	0.999	0.54
PER075	1:04:36.30	+61:22:44.9	124.509	-1.45229	2012	C star	–	–	–
PER076	1:05:16.00	+62:29:10.0	124.528	-0.34277	2011	M1.5 Ib	0.77	1.0	1.0
PER077	1:05:23.90	+62:21:24.6	124.550	-0.47103	2012	M0.5 Iab	0.845	1.0	1.0
PER078	1:06:30.00	+57:34:00.4	124.959	-5.24568	2012	M3.5 Ib – II	0.477	0.947	0.406
PER079	1:06:59.70	+63:46:23.4	124.650	0.95332	2012	G2.0 Ia	0.689	1.0	0.017
PER080	1:07:53.00	+63:25:11.6	124.770	0.60686	2012	K3.0 Iab	0.815	1.0	1.0
PER081	1:08:55.70	+61:10:54.3	125.039	-1.61842	2012	M4.5 II	0.295	0.109	0.193
PER082	1:09:13.00	+65:07:02.0	124.802	2.31005	2011	M2.0 Ib	0.77	1.0	1.0
PER083	1:09:42.20	+62:25:09.8	125.044	-0.37742	2012	M8.0 III	0.179	0.0	0.001
PER084	1:09:44.50	+57:03:52.6	125.430	-5.71832	2012	M2.0 II	0.49	1.0	0.295
PER085	1:10:20.10	+62:30:39.8	125.111	-0.28073	2012	M2.0 Iab	0.846	1.0	1.0
PER086	1:11:32.50	+56:56:20.7	125.685	-5.82514	2012	M7.5 III	0.235	0.001	0.029
PER087	1:12:57.60	+59:52:39.6	125.633	-2.88118	2012	M5.0 III	0.285	0.33	0.089
PER088	1:14:56.60	+59:42:13.3	125.897	-3.03268	2012	M9.0 III	0.088	0.0	0.001
PER089	1:15:19.20	+57:21:40.4	126.162	-5.36067	2012	M4.0 II	0.389	0.65	0.285
PER090	1:16:04.70	+58:33:48.4	126.149	-4.15432	2012	M4.0 II – III	0.396	0.081	0.321
PER091	1:16:45.00	+63:28:27.0	125.754	0.74118	2011	M0.0 Ib	0.765	1.0	1.0
PER092	1:17:48.10	+64:13:39.7	125.793	1.50252	2012	K5.0 Ib – II	0.558	1.0	0.951
PER093	1:18:13.80	+57:48:11.3	126.508	-4.88246	2012	M4.0 II	0.394	0.144	0.173
PER094	1:18:14.00	+57:48:11.0	126.508	-4.88250	2011	M5.0 II	0.381	0.108	0.221
PER095	1:18:38.00	+58:02:12.8	126.537	-4.64438	2012	M1.0 Ib – II	0.536	1.0	0.978
PER096	1:18:48.20	+59:46:41.4	126.374	-2.91057	2012	M4.0 II	0.292	0.138	0.155
PER097	1:18:52.70	+58:09:30.9	126.556	-4.51994	2012	C star	–	–	–
PER098	1:20:01.40	+57:31:29.1	126.777	-5.13341	2012	M4.5 II	0.297	0.02	0.091
PER099	1:21:09.10	+56:32:02.3	127.044	-6.10037	2012	M7.0 II	0.211	0.0	0.001
PER100	1:21:55.00	+61:20:55.0	126.578	-1.30718	2011	M7.0 III	0.085	0.0	0.04
PER101	1:22:04.10	+66:50:12.3	125.944	4.14433	2012	S star	0.347	0.072	0.451
PER102	1:22:56.30	+61:10:34.6	126.721	-1.46353	2012	K4.0 Iab	0.826	1.0	1.0
PER103	1:23:01.80	+61:59:40.7	126.632	-0.64996	2012	M1.5 Ib	0.876	1.0	1.0
PER104	1:24:25.20	+57:11:53.4	127.408	-5.38668	2012	M0.5 Ib	0.643	1.0	1.0
PER105	1:25:02.10	+61:04:41.0	126.984	-1.52907	2012	M9.0 III	0.066	0.0	0.0
PER106	1:25:09.40	+58:49:18.7	127.294	-3.76402	2012	M5.0 Ib – II	0.384	0.078	0.217
PER107	1:25:10.40	+60:52:38.0	127.027	-1.72601	2012	M1.0 Iab	0.867	1.0	1.0
PER108	1:25:22.80	+57:38:11.7	127.479	-4.93518	2012	M3.0 II	0.383	0.825	0.324

Table A1: continued.

ID	RA J2000	DEC J2000	l (deg)	b (deg)	Epoch	Visual Classification	P _{PCA}	P _{CaT}	P _{Ti/Fe}
PER109	1:25:58.30	+63:29:32.3	126.774	0.87846	2012	M3.0 Iab	0.867	1.0	1.0
PER110	1:26:43.20	+62:52:31.7	126.941	0.27868	2012	M0.5 Iab	0.796	1.0	1.0
PER111	1:29:20.60	+61:45:41.8	127.400	-0.78085	2012	M2.0 Ib	0.764	1.0	0.947
PER112	1:29:47.90	+58:47:19.3	127.895	-3.71291	2012	C star	–	–	–
PER113	1:31:34.30	+59:57:48.1	127.940	-2.51758	2012	M0.0 Ib	0.783	1.0	1.0
PER114	1:32:00.20	+62:19:44.5	127.622	-0.17273	2012	M2.0 Iab	0.867	1.0	1.0
PER115	1:33:32.60	+57:45:05.5	128.545	-4.66064	2012	C star	–	–	–
PER116	1:33:33.10	+61:33:29.6	127.925	-0.90458	2012	M0.5 Iab	0.869	1.0	1.0
PER117	1:34:07.20	+65:11:18.5	127.393	2.68709	2012	K5.0 Iab	0.748	1.0	0.984
PER118	1:34:48.50	+65:47:51.8	127.362	3.29973	2012	M5.0 III	0.381	0.087	0.237
PER119	1:34:52.20	+62:46:28.6	127.876	0.32052	2012	K5.0 Iab – Ib	0.758	1.0	1.0
PER120	1:37:52.40	+62:47:48.8	128.210	0.40199	2012	M3.0 Iab	0.922	1.0	1.0
PER121	1:38:03.50	+61:02:49.2	128.546	-1.31558	2012	K5.0 Iab – Ib	0.752	1.0	1.0
PER122	1:38:35.90	+60:49:25.7	128.651	-1.52323	2012	K5.0 Ib	0.607	1.0	0.998
PER123	1:39:19.00	+60:39:38.0	128.767	-1.66763	2011	M4.0 II	0.381	0.745	0.459
PER124	1:39:46.80	+59:42:29.2	129.000	-2.59284	2012	S star	0.591	0.969	0.726
PER125	1:39:51.60	+60:54:08.1	128.787	-1.41783	2012	M2.0 Iab	0.798	1.0	1.0
PER126	1:41:01.00	+61:31:01.0	128.808	-0.78790	2011	M4.0 III	0.37	0.066	0.439
PER127	1:42:16.40	+61:25:16.4	128.974	-0.85278	2012	K5.0 Iab – Ib	0.782	1.0	1.0
PER128	1:44:38.30	+61:37:43.0	129.208	-0.59314	2012	M0.0 Iab – Ib	0.734	1.0	1.0
PER129	1:44:49.70	+57:42:01.4	130.039	-4.43273	2012	M4.5 II	0.297	0.653	0.184
PER130	1:45:38.70	+61:02:22.7	129.448	-1.14445	2012	M0.0 Iab	0.841	1.0	1.0
PER131	1:47:44.00	+62:06:36.0	129.463	-0.04573	2011	M6.0 III	0.338	0.0	0.045
PER132	1:47:46.00	+63:50:22.0	129.093	1.64351	2012	S star	0.089	0.001	0.0
PER133	1:51:40.00	+61:20:59.0	130.088	-0.68246	2011	M2.0 Ib	0.795	1.0	1.0
PER134	1:54:01.20	+64:39:50.9	129.566	2.60149	2012	M3.0 II – III	0.382	0.911	0.272
PER135	1:55:53.20	+64:16:56.1	129.854	2.28013	2012	M4.0 II	0.381	0.774	0.398
PER136	1:56:35.80	+62:04:13.0	130.481	0.15737	2012	M1.0 Ib	0.794	1.0	1.0
PER137	1:56:41.00	+57:01:04.0	131.757	-4.73185	2011	M5.0 II	0.452	0.106	0.224
PER138	1:56:45.40	+60:49:03.8	130.813	-1.05065	2012	M1.0 Ib	0.653	1.0	1.0
PER139	1:57:40.10	+60:13:07.9	131.072	-1.60191	2012	K4.0 Ib	0.629	1.0	1.0
PER140	1:58:14.50	+59:37:01.1	131.295	-2.16562	2012	M3.0 II – III	0.426	0.765	0.122
PER141	1:58:18.50	+64:03:55.8	130.164	2.13674	2012	M5.0 III	0.198	0.0	0.074
PER142	1:58:56.60	+61:00:04.0	131.023	-0.80569	2012	M0.5 Iab	0.803	1.0	1.0
PER143	2:00:09.30	+55:45:14.1	132.550	-5.82933	2012	M5.5 II	0.279	0.034	0.09
PER144	2:00:57.00	+58:36:58.0	131.893	-3.04103	2011	M7.5 III	0.18	0.0	0.026
PER145	2:01:26.60	+64:08:37.8	130.474	2.30203	2012	M3.5 Iab	0.805	1.0	0.997
PER146	2:02:42.00	+58:04:53.0	132.259	-3.49410	2011	M4.0 III	0.185	0.0	0.021
PER147	2:03:08.20	+62:11:24.1	131.188	0.47303	2012	M0.0 Ib	0.776	1.0	1.0
PER148	2:05:05.90	+58:16:23.1	132.510	-3.22228	2012	M9.0 III	0.075	0.0	0.0
PER149	2:08:15.70	+59:15:56.0	132.617	-2.15386	2012	M7.0 Iab	0.352	0.0	0.029
PER150	2:08:54.10	+58:42:28.6	132.860	-2.66254	2012	M7.5 III	0.213	0.0	0.028
PER151	2:14:53.30	+66:29:56.6	131.127	4.96425	2012	M0.0 Ib – II	0.508	1.0	0.965
PER152	2:16:19.50	+64:52:17.4	131.791	3.46990	2012	M3.0 II	0.375	0.993	0.253
PER153	2:19:34.00	+58:23:57.0	134.279	-2.51757	2011	M7.5 III	0.144	0.0	0.0
PER154	2:19:47.00	+58:38:48.0	134.223	-2.27487	2011	K0.0 II	0.697	1.0	1.0
PER155	2:21:00.00	+57:09:30.0	134.878	-3.62148	2011	M1.5 Iab	0.855	1.0	1.0
PER156	2:22:24.20	+57:06:34.0	135.074	-3.60227	2012	M4.0 Iab	0.671	0.604	0.556
PER157	2:22:51.70	+58:35:11.2	134.621	-2.19506	2012	M3.0 Ia	0.51	0.0	0.004
PER158	2:23:39.00	+61:24:58.0	133.731	0.49281	2011	M3.0 Ib – II	0.798	1.0	1.0
PER159	2:24:29.80	+55:41:06.3	135.844	-4.83619	2012	M5.0 III	0.319	0.053	0.204
PER160	2:24:41.10	+59:57:47.2	134.358	-0.82371	2012	M4.0 II	0.501	0.987	0.669
PER161	2:26:02.70	+65:13:51.6	132.634	4.15678	2012	K0.0 Ib	0.605	1.0	1.0
PER162	2:27:49.00	+57:05:52.0	135.767	-3.35271	2011	M5.0 II	0.427	0.022	0.131
PER163	2:28:02.70	+59:46:10.0	134.821	-0.85346	2012	M2.0 II	0.501	0.995	0.286
PER164	2:28:13.00	+58:37:09.0	135.261	-1.91656	2011	M7.0 III	0.371	0.0	0.005
PER165	2:29:14.00	+61:25:53.7	134.348	0.74659	2012	M3.5 II	0.323	0.444	0.351

Table A1: continued.

ID	RA J2000	DEC J2000	l (deg)	b (deg)	Epoch	Visual Classification	P _{PCA}	P _{CaT}	P _{Ti/Fe}
PER166	2:29:51.00	+59:58:58.0	134.954	-0.57185	2011	M1.5 Iab	0.802	1.0	1.0
PER167	2:30:27.50	+62:31:45.6	134.075	1.81948	2012	M7.0 III	0.177	0.0	0.0
PER168	2:31:04.00	+56:50:26.0	136.274	-3.42795	2011	M0.0 Ib	0.78	1.0	1.0
PER169	2:32:27.90	+54:18:12.9	137.421	-5.70136	2012	M7.5 II	0.177	0.0	0.002
PER170	2:35:44.60	+65:08:58.7	133.610	4.46314	2012	M9.5 III	0.017	0.0	0.0
PER171	2:36:11.30	+60:22:41.3	135.531	0.09430	2012	M7.0 III	0.232	0.0	0.006
PER172	2:37:33.20	+54:27:48.0	138.044	-5.26506	2012	M4.0 II	0.29	0.119	0.098
PER173	2:38:43.00	+55:45:59.4	137.672	-4.00450	2012	C star	–	–	–
PER174	2:39:22.90	+60:42:40.0	135.759	0.55608	2012	M7.0 III	0.182	0.0	0.012
PER175	2:41:04.90	+62:17:31.9	135.300	2.08286	2012	M8.0 II	0.114	0.0	0.001
PER176	2:41:07.80	+55:12:59.8	138.210	-4.36778	2012	M8.0 III	0.081	0.0	0.0
PER177	2:42:39.20	+66:35:04.9	133.675	6.06114	2012	M4.5 II	0.288	0.316	0.079
PER178	2:42:56.90	+60:12:16.2	136.367	0.27429	2012	K5.0 Iab	0.735	1.0	1.0
PER179	2:43:45.10	+60:25:25.0	136.366	0.51492	2012	C star	–	–	–
PER180	2:44:19.00	+60:55:55.6	136.215	1.00546	2012	M7.0 II – III	0.269	0.0	0.078
PER181	2:44:30.30	+65:42:52.7	134.213	5.35040	2012	M3.0 Ib – II	0.611	0.97	0.552
PER182	2:45:12.20	+58:05:24.5	137.518	-1.52304	2012	M0.0 Iab	0.751	1.0	1.0
PER183	2:45:39.10	+59:17:34.4	137.060	-0.40942	2012	M4.0 II	0.406	0.416	0.231
PER184	2:46:00.70	+58:45:20.1	137.331	-0.87579	2012	M5.0 Ib	0.351	0.169	0.364
PER185	2:46:21.10	+53:09:46.7	139.773	-5.90966	2012	K2.0 II	0.504	1.0	0.841
PER186	2:46:23.00	+64:19:44.0	134.986	4.18130	2011	M8.0 Ib – II	0.108	0.0	0.165
PER187	2:46:31.40	+59:35:23.9	137.033	-0.09347	2012	K2.0 Ib	0.627	1.0	1.0
PER188	2:46:40.00	+63:00:19.8	135.583	2.99950	2012	M6.0 III	0.338	0.001	0.093
PER189	2:47:52.50	+64:45:17.0	134.946	4.63461	2012	M3.0 II	0.504	0.989	0.68
PER190	2:49:07.00	+60:13:11.0	137.054	0.61494	2011	M2.0 Ib	0.697	1.0	0.999
PER191	2:49:54.00	+61:02:09.0	136.782	1.39051	2011	M3.0 Ib	0.917	1.0	1.0
PER192	2:50:14.00	+62:25:14.0	136.207	2.65093	2011	M3.5 Ib	0.892	1.0	1.0
PER193	2:50:39.50	+58:53:08.4	137.816	-0.49729	2012	C star	–	–	–
PER194	2:50:57.00	+60:44:27.0	137.027	1.18225	2011	M6.0 Ib – II	0.401	0.084	0.177
PER195	2:52:42.00	+58:42:49.5	138.129	-0.53329	2012	M5.0 Ib – II	0.237	0.0	0.091
PER196	2:52:52.90	+54:24:34.2	140.091	-4.36578	2012	C star	–	–	–
PER197	2:54:19.00	+59:29:14.1	137.965	0.25050	2012	C star	–	–	–
PER198	2:55:30.00	+60:13:59.0	137.756	0.98184	2011	M2.0 Iab	0.802	1.0	1.0
PER199	2:56:19.60	+58:52:18.8	138.475	-0.17861	2012	M0.5 II	0.524	1.0	0.981
PER200	2:56:53.20	+57:33:24.9	139.149	-1.31053	2012	M2.0 Iab	0.841	1.0	1.0
PER201	2:59:17.80	+51:50:24.5	142.141	-6.19853	2012	M6.5 III	0.213	0.006	0.175
PER202	21:26:36.8	+59:08:42.4	99.230	6.05462	2012	M8.0 III	0.151	0.0	0.01
PER203	21:37:03.0	+54:55:40.8	97.384	2.00469	2012	M4.5 II – III	0.479	0.439	0.453
PER204	21:40:39.0	+54:19:28.7	97.374	1.20759	2012	M7.0 II – III	0.325	0.0	0.011
PER205	21:41:08.1	+58:15:56.8	100.023	4.12973	2012	M0.0 II	0.648	0.995	0.71
PER206	21:42:08.8	+54:58:02.1	97.959	1.55022	2012	M4.5 III	0.423	0.207	0.357
PER207	21:42:16.0	+54:38:43.7	97.762	1.29558	2012	C star	–	–	–
PER208	21:44:04.3	+53:42:11.6	97.348	0.40877	2012	K2.0 Ia	0.78	1.0	1.0
PER209	21:47:17.2	+54:21:13.8	98.129	0.60149	2012	M0.0 II	0.552	1.0	0.571
PER210	21:48:39.6	+52:54:07.0	97.358	-0.64564	2012	M4.0 Iab	0.576	0.623	0.343
PER211	21:49:30.2	+53:22:11.5	97.753	-0.36488	2012	M3.0 II	0.401	0.999	0.416
PER212	21:50:00.6	+53:23:41.5	97.827	-0.39344	2012	M5.0 III	0.308	0.301	0.237
PER213	21:50:18.2	+52:38:15.6	97.382	-1.00762	2012	C star	–	–	–
PER214	21:51:30.3	+54:44:27.0	98.847	0.51209	2012	M6.0 III	0.129	0.0	0.0
PER215	21:51:31.0	+54:49:10.8	98.898	0.57231	2012	M0.5 II	0.541	1.0	0.659
PER216	21:51:38.0	+54:45:38.0	98.874	0.51578	2011	M6.0 Ib – II	0.37	0.093	0.279
PER217	21:51:47.5	+55:08:10.5	99.127	0.79368	2012	M5.0 III	0.393	0.03	0.181
PER218	21:51:48.3	+55:05:12.1	99.098	0.75393	2012	C star	–	–	–
PER219	21:52:12.1	+54:49:46.2	98.981	0.51799	2012	M2.0 Ib – II	0.593	1.0	0.739
PER220	21:52:19.9	+52:53:14.6	97.778	-1.00687	2012	M2.0 II	0.471	0.991	0.633
PER221	21:52:36.0	+55:58:38.0	99.744	1.37687	2011	M6.0 Ib – II	0.5	0.001	0.057
PER222	21:52:44.9	+55:17:36.2	99.332	0.83052	2012	M4.0 II	0.401	0.875	0.499

Table A1: continued.

ID	RA J2000	DEC J2000	l (deg)	b (deg)	Epoch	Visual Classification	P _{PCA}	P _{CaT}	P _{Ti/Fe}
PER223	21:52:59.3	+52:54:56.0	97.873	-1.04690	2012	M2.0 II – III	0.463	0.999	0.391
PER224	21:53:03.6	+62:02:14.6	103.599	6.06086	2012	M5.0 III	0.341	0.029	0.193
PER225	21:53:41.3	+59:17:33.0	101.933	3.87295	2012	M5.0 III	0.494	0.169	0.234
PER226	21:53:53.4	+53:18:45.6	98.226	-0.82097	2012	M0.5 II	0.498	1.0	0.852
PER227	21:54:14.5	+52:40:50.6	97.874	-1.34862	2012	M4.5 II	0.437	0.319	0.325
PER228	21:54:16.9	+58:33:20.8	101.533	3.24922	2012	M2.0 II	0.523	1.0	0.207
PER229	21:54:24.6	+54:15:52.5	98.878	-0.12324	2012	M4.5 II – III	0.325	0.395	0.317
PER230	21:54:28.0	+53:43:51.8	98.553	-0.54658	2012	M4.5 II	0.3	0.178	0.258
PER231	21:54:30.8	+56:04:00.3	100.009	1.28014	2012	K3.0 II	0.443	0.982	0.694
PER232	21:55:05.2	+54:29:01.5	99.091	-0.01242	2012	C star	–	–	–
PER233	21:55:07.9	+52:04:10.6	97.602	-1.91211	2012	M7.0 II – III	0.315	0.0	0.051
PER234	21:55:23.2	+53:34:57.2	98.568	-0.74760	2012	M1.0 Ib	0.858	1.0	1.0
PER235	21:55:40.0	+53:58:03.0	98.839	-0.47054	2011	K4.0 Iab – Ib	0.873	1.0	1.0
PER236	21:55:43.0	+52:31:09.0	97.950	-1.61421	2011	M4.0 II	0.299	0.289	0.33
PER237	21:55:49.0	+54:00:05.4	98.877	-0.45741	2012	M7.5 III	0.185	0.0	0.003
PER238	21:55:54.7	+53:59:04.7	98.878	-0.47929	2012	K4.0 Ib	0.683	1.0	0.997
PER239	21:56:09.8	+59:30:33.1	102.316	3.84717	2012	M3.5 II	0.443	0.649	0.371
PER240	21:56:27.7	+53:46:19.4	98.811	-0.69667	2012	M4.0 II	0.405	0.081	0.037
PER241	21:57:04.2	+59:06:17.7	102.157	3.45747	2012	M5.0 Ib – II	0.426	0.01	0.145
PER242	21:57:50.2	+54:53:58.9	99.661	0.07092	2012	C star	–	–	–
PER243	21:57:52.9	+52:52:39.4	98.429	-1.53309	2012	M7.0 Ib	0.431	0.007	0.093
PER244	21:58:15.9	+55:07:05.2	99.843	0.20633	2012	M1.0 Ib – II	0.656	1.0	0.929
PER245	21:58:50.2	+52:00:58.8	98.019	-2.30413	2012	M5.5 III	0.319	0.002	0.085
PER246	21:59:28.3	+56:14:17.8	100.659	0.99161	2012	M2.0 II	0.605	0.996	0.723
PER247	21:59:40.7	+53:10:29.2	98.825	-1.46193	2012	M4.5 II	0.485	0.378	0.345
PER248	22:00:03.1	+61:16:25.3	103.780	4.94768	2012	K2.0 Ib	0.671	1.0	1.0
PER249	22:00:10.0	+52:54:16.0	98.719	-1.72147	2011	M6.0 Ib – II	0.39	0.026	0.114
PER250	22:00:45.7	+54:54:47.0	100.003	-0.17381	2012	M2.0 Ib – II	0.447	1.0	0.664
PER251	22:01:00.8	+51:17:20.6	97.846	-3.08719	2012	M0.5 Ib	0.614	1.0	0.899
PER252	22:01:04.6	+54:29:16.1	99.783	-0.54055	2012	M6.0 III	0.316	0.011	0.12
PER253	22:02:53.1	+56:50:09.9	101.395	1.18558	2012	M4.0 II	0.465	0.32	0.313
PER254	22:02:55.7	+54:14:00.5	99.846	-0.90583	2012	M3.0 II	0.521	0.971	0.572
PER255	22:03:04.9	+51:39:29.4	98.326	-2.98537	2012	M5.5 III	0.268	0.001	0.083
PER256	22:03:12.1	+55:06:56.8	100.404	-0.22134	2012	M8.0 III	0.13	0.0	0.016
PER257	22:05:09.0	+63:04:48.2	105.348	6.03446	2012	M5.5 III	0.455	0.025	0.142
PER258	22:05:28.4	+62:30:10.3	105.034	5.54783	2012	M7.0 III	0.189	0.0	0.04
PER259	22:05:32.6	+63:02:37.9	105.363	5.97889	2012	M5.0 III	0.29	0.175	0.153
PER260	22:05:37.9	+53:55:59.9	99.987	-1.38265	2012	M7.5 Ib – II	0.373	0.001	0.04
PER261	22:05:48.5	+58:45:40.0	102.851	2.50429	2012	M0.5 II	0.585	0.998	0.143
PER262	22:05:49.5	+53:37:44.3	99.831	-1.64540	2012	M5.0 III	0.459	0.156	0.189
PER263	22:06:10.7	+51:49:35.1	98.812	-3.13410	2012	M4.0 II	0.342	0.675	0.323
PER264	22:06:17.0	+55:00:17.4	100.694	-0.57187	2012	M7.0 II – III	0.404	0.0	0.024
PER265	22:06:17.1	+52:59:16.3	99.509	-2.20427	2012	M7.5 Ib – II	0.258	0.0	0.015
PER266	22:06:20.9	+55:53:33.7	101.223	0.14141	2012	K3.0 Ib	0.567	1.0	1.0
PER267	22:06:21.0	+59:39:38.1	103.438	3.19065	2012	M2.0 Iab	0.852	1.0	1.0
PER268	22:06:36.5	+55:29:55.9	101.022	-0.19902	2012	M3.0 Ib – II	0.589	1.0	0.724
PER269	22:06:37.7	+59:41:20.2	103.483	3.19296	2012	M4.0 Ib	0.782	0.636	0.786
PER270	22:07:03.7	+57:22:58.0	102.176	1.29127	2012	M4.0 III	0.318	0.703	0.249
PER271	22:07:30.0	+53:04:02.3	99.704	-2.24693	2012	M3.0 II	0.445	0.998	0.358
PER272	22:08:12.0	+56:30:47.0	101.795	0.49434	2011	M6.0 II	0.301	0.0	0.049
PER273	22:08:12.7	+55:55:03.7	101.450	0.00910	2012	M3.0 II	0.529	0.956	0.393
PER274	22:08:38.4	+59:33:01.3	103.608	2.93190	2012	M1.0 Ia	0.885	1.0	1.0
PER275	22:08:41.9	+51:45:14.1	99.086	-3.42081	2012	M6.0 III	0.327	0.001	0.038
PER276	22:08:42.3	+53:26:04.9	100.065	-2.05323	2012	M7.0 II – III	0.231	0.0	0.009
PER277	22:09:33.2	+60:53:54.2	104.484	3.96419	2012	M4.0 II	0.4	0.25	0.195
PER278	22:09:37.0	+52:09:49.0	99.440	-3.16903	2012	M5.0 III	0.37	0.031	0.08
PER279	22:09:43.7	+51:26:13.9	99.033	-3.77161	2012	M4.0 II	0.332	0.558	0.127

Table A1: continued.

ID	RA J2000	DEC J2000	l (deg)	b (deg)	Epoch	Visual Classification	P _{PCA}	P _{CaT}	P _{Ti/Fe}
PER280	22:09:49.0	+52:05:06.7	99.419	-3.25076	2012	M5.0 III	0.274	0.022	0.047
PER281	22:10:20.0	+56:11:49.0	101.853	0.06556	2011	M1.5 Ib	0.77	1.0	1.0
PER282	22:10:22.0	+56:28:54.0	102.020	0.29578	2011	M8.0 III	0.078	0.0	0.0
PER283	22:11:00.5	+55:05:33.2	101.296	-0.89319	2012	M1.0 Ib	0.673	1.0	1.0
PER284	22:11:11.0	+55:16:54.0	101.425	-0.75253	2011	M8.0 III	0.022	0.0	0.0
PER285	22:11:25.0	+56:34:34.0	102.193	0.29008	2011	M2.0 Ib	0.739	1.0	1.0
PER286	22:11:35.6	+55:16:04.4	101.465	-0.79725	2012	M2.0 Ib	0.782	1.0	0.999
PER287	22:12:33.0	+57:17:03.0	102.724	0.78342	2011	M2.0 Iab	0.848	1.0	1.0
PER288	22:12:53.8	+54:12:29.6	101.016	-1.77523	2012	M3.5 III	0.263	0.672	0.263
PER289	22:13:00.0	+57:34:59.0	102.944	0.99498	2011	M3.0 II – III	0.294	0.652	0.232
PER290	22:13:09.2	+54:37:15.7	101.281	-1.45655	2012	M6.5 III	0.24	0.0	0.095
PER291	22:13:41.6	+54:19:35.4	101.179	-1.74372	2012	M2.0 III	0.545	0.796	0.215
PER292	22:13:45.7	+52:19:21.4	100.052	-3.40175	2012	M3.0 Ib – II	0.453	0.978	0.393
PER293	22:13:53.8	+55:22:01.2	101.791	-0.90188	2012	M1.0 Iab	0.618	1.0	0.919
PER294	22:14:05.8	+55:04:28.2	101.650	-1.15942	2012	M4.5 II	0.364	0.283	0.269
PER295	22:14:15.4	+59:22:00.8	104.089	2.37290	2012	M4.0 II – III	0.284	0.19	0.283
PER296	22:14:29.4	+55:50:14.8	102.126	-0.56062	2012	M1.0 Ib	0.579	1.0	1.0
PER297	22:14:33.9	+55:13:51.7	101.793	-1.06781	2012	M4.0 II	0.348	0.346	0.235
PER298	22:14:43.2	+56:20:22.4	102.435	-0.16356	2012	M2.0 Ib – II	0.479	0.997	0.589
PER299	22:15:17.6	+54:11:52.3	101.299	-1.98160	2012	M6.0 III	0.314	0.001	0.089
PER300	22:15:42.0	+57:53:06.0	103.412	1.04139	2011	M0.0 Iab	0.812	1.0	1.0
PER301	22:16:08.0	+52:29:47.4	100.450	-3.46146	2012	M4.5 II – III	0.357	0.944	0.244
PER302	22:16:20.9	+53:34:32.9	101.080	-2.58418	2012	M8.0 III	0.188	0.0	0.001
PER303	22:16:24.5	+57:23:59.5	103.219	0.58598	2012	K4.0 Iab – Ib	0.792	1.0	1.0
PER304	22:16:25.4	+54:01:18.4	101.338	-2.22018	2012	C star	–	–	–
PER305	22:16:55.4	+50:05:23.0	99.204	-5.52681	2012	M5.0 Ib – II	0.433	0.026	0.15
PER306	22:17:16.5	+56:47:15.4	102.977	0.01160	2012	M4.0 II – III	0.396	0.671	0.268
PER307	22:18:31.1	+58:39:40.9	104.151	1.48141	2012	M1.5 II	0.49	0.998	0.623
PER308	22:19:27.6	+51:09:43.9	100.137	-4.85686	2012	M5.0 III	0.397	0.006	0.103
PER309	22:19:40.6	+53:09:45.9	101.266	-3.20287	2012	M2.0 II	0.378	0.971	0.212
PER310	22:19:41.3	+50:33:20.0	99.832	-5.38342	2012	M5.0 Ib – II	0.383	0.062	0.198
PER311	22:19:45.7	+54:42:16.3	102.121	-1.91968	2012	M7.0 II	0.289	0.002	0.062
PER312	22:19:55.5	+53:39:45.2	101.571	-2.80491	2012	M5.5 III	0.362	0.067	0.143
PER313	22:19:56.5	+50:39:18.2	99.921	-5.32234	2012	M3.0 II	0.269	1.0	0.563
PER314	22:20:10.8	+56:02:24.2	102.901	-0.83367	2012	M3.5 Ib	0.786	1.0	0.987
PER315	22:20:22.0	+54:15:09.6	101.948	-2.34614	2012	M7.5 II – III	0.225	0.0	0.003
PER316	22:20:37.7	+55:42:59.0	102.777	-1.13931	2012	M4.0 III	0.432	0.463	0.173
PER317	22:20:49.0	+52:50:49.6	101.237	-3.56093	2012	M8.0 II – III	0.218	0.0	0.013
PER318	22:21:08.8	+54:27:06.4	102.152	-2.24097	2012	M4.0 II – III	0.353	0.778	0.365
PER319	22:21:11.3	+51:19:54.2	100.457	-4.86296	2012	M8.0 II	0.155	0.0	0.001
PER320	22:21:29.1	+60:43:11.6	105.591	3.00055	2012	C star	–	–	–
PER321	22:21:59.0	+55:18:03.0	102.713	-1.59247	2011	M6.0 II – III	0.352	0.0	0.018
PER322	22:22:26.9	+57:11:32.2	103.788	-0.03470	2012	M10.0 III	0.081	0.0	0.0
PER323	22:22:30.1	+55:10:55.4	102.711	-1.73234	2012	M5.0 III	0.305	0.188	0.255
PER324	22:22:34.0	+57:15:04.0	103.833	0.00625	2011	M2.0 Iab	0.808	1.0	1.0
PER325	22:23:13.6	+56:08:53.3	103.317	-0.97265	2012	M4.0 Iab	0.581	0.944	0.411
PER326	22:23:34.1	+57:39:03.0	104.161	0.27119	2012	M4.0 II	0.363	0.709	0.19
PER327	22:23:54.4	+58:14:28.6	104.515	0.74614	2012	K3.0 Ib	0.72	1.0	0.999
PER328	22:24:06.0	+57:33:37.8	104.173	0.15679	2012	M6.0 II	0.366	0.004	0.073
PER329	22:24:56.5	+58:39:03.8	104.848	1.02084	2012	M2.0 Iab	0.774	1.0	1.0
PER330	22:25:04.8	+58:36:13.2	104.838	0.97112	2012	M3.0 Ib	0.642	1.0	0.966
PER331	22:25:15.8	+57:10:15.3	104.099	-0.25655	2012	K5.0 Ib	0.736	1.0	1.0
PER332	22:25:34.9	+54:38:50.3	102.800	-2.42081	2012	M3.5 II	0.423	0.873	0.254
PER333	22:25:55.6	+56:38:52.5	103.899	-0.74830	2012	M0.0 Iab	0.764	1.0	1.0
PER334	22:26:28.5	+58:15:41.0	104.812	0.58406	2012	M3.0 II	0.4	0.963	0.079
PER335	22:26:28.8	+58:42:27.8	105.048	0.96327	2012	M5.0 III	0.431	0.07	0.174
PER336	22:26:40.0	+58:31:34.0	104.973	0.79602	2011	M7.0 III	0.187	0.002	0.147

Table A1: continued.

ID	RA J2000	DEC J2000	l (deg)	b (deg)	Epoch	Visual Classification	P _{PCA}	P _{CaT}	P _{Ti/Fe}
PER337	22:26:52.7	+60:09:54.4	105.857	2.17639	2012	K3.0 Ib	0.687	1.0	0.999
PER338	22:27:05.3	+53:29:22.0	102.377	-3.52117	2012	M2.0 Ib	0.661	1.0	0.965
PER339	22:27:22.6	+57:15:59.0	104.392	-0.32604	2012	M9.0 III	0.069	0.0	0.0
PER340	22:27:29.4	+59:26:01.7	105.539	1.51329	2012	M1.0 Iab	0.899	1.0	1.0
PER341	22:27:55.9	+52:49:15.6	102.133	-4.15672	2012	M2.0 III	0.474	0.948	0.229
PER342	22:28:13.4	+57:42:44.2	104.722	-0.00510	2012	M3.0 II	0.486	0.997	0.56
PER343	22:28:17.4	+59:14:04.1	105.522	1.29002	2012	M3.0 Iab	0.913	1.0	1.0
PER344	22:28:53.6	+58:01:07.3	104.958	0.21041	2012	M4.5 II	0.387	0.184	0.193
PER345	22:29:11.2	+57:12:46.7	104.574	-0.49910	2012	M1.0 Ib – II	0.56	1.0	0.905
PER346	22:29:26.7	+59:06:24.4	105.582	1.10409	2012	M5.0 III	0.334	0.051	0.285
PER347	22:29:37.8	+59:30:15.6	105.808	1.43228	2012	M2.0 Iab	0.899	1.0	1.0
PER348	22:29:54.1	+56:27:25.5	104.267	-1.19684	2012	M4.0 II	0.334	0.172	0.209
PER349	22:30:02.4	+57:03:12.8	104.591	-0.69539	2012	M4.5 II	0.424	0.311	0.375
PER350	22:30:27.3	+57:21:51.0	104.799	-0.45790	2012	M2.0 Ib	0.671	1.0	0.941
PER351	22:30:41.7	+54:53:51.5	103.560	-2.59168	2012	M2.0 Ib – II	0.563	1.0	0.864
PER352	22:31:28.9	+64:41:50.6	108.672	5.77415	2012	M3.0 II	0.478	0.999	0.531
PER353	22:31:41.0	+59:00:43.6	105.781	0.87516	2012	M4.0 II	0.413	0.261	0.221
PER354	22:31:50.1	+56:59:48.9	104.771	-0.86912	2012	M6.0 II	0.286	0.002	0.026
PER355	22:32:25.5	+59:32:58.4	106.136	1.28973	2012	C star	–	–	–
PER356	22:32:26.8	+58:37:05.8	105.666	0.48580	2012	C star	–	–	–
PER357	22:32:31.0	+59:36:23.4	106.175	1.33291	2012	M3.0 Iab	0.906	1.0	1.0
PER358	22:33:00.0	+57:38:04.3	105.230	-0.39948	2012	M2.0 Ib – II	0.376	1.0	0.745
PER359	22:33:01.2	+55:16:14.9	104.037	-2.44016	2012	M3.0 III	0.354	0.674	0.194
PER360	22:33:05.0	+58:28:42.0	105.666	0.32307	2011	K1.0 Ib	0.596	1.0	0.959
PER361	22:33:23.8	+55:27:41.0	104.180	-2.30273	2012	M4.0 II	0.489	0.891	0.423
PER362	22:33:34.6	+58:53:47.0	105.933	0.65170	2012	M3.5 Ib	0.825	1.0	1.0
PER363	22:33:46.0	+58:16:59.3	105.645	0.10935	2012	M7.5 II – III	0.234	0.0	0.0
PER364	22:33:49.3	+57:29:48.8	105.256	-0.57389	2012	M3.0 III	0.29	0.301	0.204
PER365	22:34:09.3	+58:59:26.1	106.045	0.69563	2012	K5.0 Iab	0.853	1.0	1.0
PER366	22:34:10.4	+56:59:27.4	105.043	-1.03526	2012	M5.0 II	0.286	0.003	0.056
PER367	22:34:58.0	+55:55:53.0	104.607	-2.00732	2011	M6.0 Ib – II	0.416	0.003	0.113
PER368	22:35:15.3	+58:17:13.3	105.817	0.01478	2012	M1.0 II	0.588	0.99	0.272
PER369	22:35:29.7	+56:19:56.5	104.871	-1.69645	2012	S star	0.62	1.0	0.287
PER370	22:35:40.5	+55:29:25.1	104.474	-2.43944	2012	M5.0 II – III	0.529	0.255	0.224
PER371	22:35:54.4	+58:39:28.6	106.075	0.29424	2012	M5.0 II – III	0.346	0.202	0.083
PER372	22:36:13.0	+52:59:04.1	103.295	-4.65318	2012	M9.0 III	0.029	0.0	0.008
PER373	22:36:51.8	+52:37:05.0	103.198	-5.01984	2012	M9.0 III	0.025	0.0	0.0
PER374	22:37:35.9	+61:16:09.1	107.548	2.46072	2012	M5.0 Ib	0.579	0.002	0.104
PER375	22:37:44.2	+60:22:22.5	107.123	1.67154	2012	M2.0 Iab	0.877	1.0	1.0
PER376	22:38:04.4	+55:36:27.2	104.827	-2.50485	2012	M0.5 Ib – II	0.558	1.0	0.969
PER377	22:38:24.7	+58:28:54.8	106.273	-0.01973	2012	C star	–	–	–
PER378	22:38:51.3	+56:26:58.2	105.334	-1.82339	2012	M0.5 Ib	0.688	1.0	1.0
PER379	22:38:51.8	+54:21:07.7	104.312	-3.65559	2012	M6.0 III	0.26	0.0	0.004
PER380	22:39:20.6	+60:10:28.8	107.200	1.40132	2012	M5.0 III	0.309	0.092	0.125
PER381	22:39:42.9	+55:30:38.6	104.983	-2.70246	2012	M2.0 II	0.617	1.0	0.763
PER382	22:39:45.3	+57:36:52.8	106.007	-0.86404	2012	M5.0 III	0.278	0.111	0.18
PER383	22:39:58.5	+57:20:19.1	105.899	-1.11997	2012	M1.0 II	0.2	0.0	0.0
PER384	22:40:10.8	+59:57:18.1	107.185	1.15860	2012	M1.0 II	0.546	0.29	0.562
PER385	22:40:12.1	+59:24:55.6	106.927	0.68461	2012	M7.5 III	0.276	0.0	0.02
PER386	22:41:00.0	+58:44:20.1	106.692	0.04214	2012	M6.0 III	0.314	0.0	0.02
PER387	22:41:11.7	+59:27:59.0	107.063	0.66860	2012	K2.0 Ib	0.73	1.0	0.994
PER388	22:41:27.0	+56:39:09.0	105.745	-1.81818	2011	M8.0 III	0.052	0.0	0.02
PER389	22:42:02.8	+58:04:05.4	106.492	-0.61257	2012	M3.5 II	0.471	0.933	0.442
PER390	22:42:20.0	+56:47:52.0	105.921	-1.74828	2011	M2.0 Iab – Ib	0.862	1.0	1.0
PER391	22:43:03.7	+59:44:03.4	107.398	0.79180	2012	M0.0 II	0.469	1.0	0.32
PER392	22:43:14.0	+59:45:09.0	107.425	0.79764	2011	M5.0 Ib	0.864	0.937	0.904
PER393	22:44:09.7	+54:58:18.9	105.283	-3.47840	2012	M7.0 II	0.312	0.0	0.006

Table A1: continued.

ID	RA J2000	DEC J2000	l (deg)	b (deg)	Epoch	Visual Classification	P _{PCA}	P _{CaT}	P _{Ti/Fe}
PER394	22:45:04.2	+56:37:18.6	106.170	-2.08036	2012	C star	–	–	–
PER395	22:45:23.4	+55:27:27.5	105.666	-3.13114	2012	M3.0 II	0.484	1.0	0.681
PER396	22:45:32.3	+55:12:47.9	105.571	-3.35718	2012	M9.0 III	0.09	0.0	0.0
PER397	22:45:44.3	+58:57:02.6	107.332	-0.06029	2012	M5.0 III	0.389	0.012	0.059
PER398	22:45:46.9	+60:35:20.4	108.097	1.38842	2012	K5.0 Ib	0.766	1.0	1.0
PER399	22:47:26.6	+58:18:31.6	107.233	-0.73222	2012	M0.0 II – III	0.589	1.0	0.09
PER400	22:47:46.1	+55:18:13.0	105.895	-3.42380	2012	C star	–	–	–
PER401	22:48:58.1	+55:38:57.0	106.204	-3.19380	2012	M1.0 Ib – II	0.539	1.0	0.9
PER402	22:49:03.6	+58:52:04.0	107.675	-0.33062	2012	M3.0 Ib – II	0.533	0.807	0.386
PER403	22:49:10.4	+59:18:12.9	107.886	0.05136	2012	M2.0 Iab	0.865	1.0	0.997
PER404	22:49:33.1	+58:58:09.6	107.778	-0.26873	2012	M2.0 II	0.545	0.987	0.695
PER405	22:49:38.9	+57:33:31.7	107.153	-1.53324	2012	M4.0 II	0.415	0.762	0.485
PER406	22:49:59.0	+60:17:57.0	108.426	0.89385	2011	K2.0 Ia	0.846	1.0	1.0
PER407	22:50:06.9	+57:31:37.6	107.194	-1.58973	2012	C star	–	–	–
PER408	22:50:08.3	+55:36:48.6	106.335	-3.30026	2012	M7.5 Ib – II	0.336	0.002	0.103
PER409	22:50:22.9	+57:29:08.6	107.208	-1.64280	2012	K3.0 Ib	0.675	1.0	1.0
PER410	22:50:50.9	+53:21:14.8	105.409	-5.36490	2012	M4.5 II – III	0.297	0.248	0.239
PER411	22:50:53.1	+61:45:57.8	109.182	2.15594	2012	M4.0 Ib	0.792	0.98	0.938
PER412	22:51:02.1	+55:45:19.9	106.512	-3.23001	2012	M0.0 Ib – II	0.594	1.0	0.987
PER413	22:51:04.1	+57:57:37.0	107.502	-1.25945	2012	M3.5 II	0.418	0.72	0.37
PER414	22:51:17.9	+57:25:58.4	107.294	-1.74518	2012	M1.5 II	0.465	0.999	0.766
PER415	22:51:29.7	+52:23:52.1	105.066	-6.26351	2012	M0.5 II	0.466	1.0	0.633
PER416	22:51:34.5	+58:00:10.3	107.581	-1.25124	2012	M3.5 II	0.289	0.436	0.234
PER417	22:51:59.1	+56:55:44.2	107.154	-2.23795	2012	M2.0 II	0.419	1.0	0.724
PER418	22:51:59.3	+63:22:56.1	110.016	3.54623	2012	M2.0 II	0.43	0.975	0.639
PER419	22:53:12.3	+61:17:00.3	109.216	1.60074	2012	M3.0 Ib	0.837	1.0	1.0
PER420	22:53:18.1	+58:58:33.7	108.214	-0.47779	2012	K2.0 Ib	0.694	1.0	1.0
PER421	22:54:01.2	+60:47:41.7	109.090	1.11835	2012	M1.5 Iab	0.792	1.0	0.999
PER422	22:54:16.0	+60:49:28.9	109.130	1.13204	2012	M3.0 Iab – Ib	0.77	1.0	0.987
PER423	22:54:30.4	+60:47:50.5	109.145	1.09469	2012	M0.5 Ib	0.81	1.0	1.0
PER424	22:54:31.2	+57:25:58.2	107.684	-1.93610	2012	M7.0 Ib – II	0.267	0.0	0.066
PER425	22:54:45.1	+60:46:42.2	109.164	1.06462	2012	C star	–	–	–
PER426	22:55:38.6	+55:50:43.9	107.135	-3.43365	2012	M3.5 II – III	0.296	0.391	0.377
PER427	22:56:07.3	+54:13:45.5	106.498	-4.92150	2012	C star	–	–	–
PER428	22:56:36.8	+61:31:08.1	109.685	1.63618	2012	M4.0 Iab	0.69	0.97	0.82
PER429	22:57:00.3	+57:39:59.6	108.085	-1.86870	2012	M7.5 III	0.183	0.0	0.094
PER430	22:57:04.9	+57:40:43.6	108.100	-1.86202	2012	K3.0 Ib	0.736	1.0	1.0
PER431	22:57:16.3	+58:17:16.8	108.382	-1.32148	2012	M0.0 II	0.526	0.992	0.972
PER432	22:57:20.2	+56:22:04.2	107.573	-3.06293	2012	C star	–	–	–
PER433	22:57:40.9	+58:49:12.7	108.657	-0.86235	2012	M2.0 II – III	0.433	0.0	0.489
PER434	22:58:16.0	+56:58:33.0	107.946	-2.56642	2011	M5.0 Ib – II	0.341	0.147	0.27
PER435	22:59:50.9	+66:21:19.2	112.058	5.86840	2012	M4.0 II	0.339	0.162	0.262
PER436	23:00:17.4	+56:08:49.3	107.852	-3.43576	2012	M9.0 III	0.121	0.0	0.004
PER437	23:01:03.2	+56:53:33.2	108.257	-2.80079	2012	M0.5 Ib – II	0.493	1.0	0.976
PER438	23:01:04.2	+56:58:30.1	108.294	-2.72661	2012	M3.0 Ib – II	0.433	0.853	0.534
PER439	23:01:07.0	+61:02:52.0	109.979	0.98146	2011	M2.0 Iab	0.8	1.0	1.0
PER440	23:02:24.0	+58:14:12.4	108.974	-1.64900	2012	K2.0 Ib	0.589	1.0	0.998
PER441	23:02:59.5	+64:12:44.3	111.472	3.78070	2012	M1.5 Ib – II	0.483	0.985	0.401
PER442	23:04:31.7	+64:08:44.3	111.598	3.65215	2012	M2.0 Ib	0.84	1.0	1.0
PER443	23:04:38.3	+58:34:41.4	109.380	-1.45511	2012	M7.5 Iab	0.294	0.0	0.004
PER444	23:04:49.6	+56:32:57.6	108.591	-3.32473	2012	M7.5 II	0.269	0.0	0.04
PER445	23:06:07.2	+59:25:05.1	109.889	-0.76018	2012	M2.0 Ib – II	0.439	1.0	0.547
PER446	23:06:27.2	+60:53:05.6	110.506	0.57152	2012	M1.0 Iab	0.802	1.0	1.0
PER447	23:06:54.8	+60:33:26.0	110.429	0.24810	2012	M0.5 Iab	0.901	1.0	1.0
PER448	23:06:56.4	+60:54:16.4	110.568	0.56637	2012	M3.0 II	0.429	0.967	0.404
PER449	23:08:04.7	+55:42:56.6	108.679	-4.26942	2012	M5.5 III	0.402	0.006	0.05
PER450	23:08:39.8	+58:18:09.9	109.757	-1.91535	2012	M7.0 Ib – II	0.327	0.001	0.053

Table A1: continued.

ID	RA J2000	DEC J2000	l (deg)	b (deg)	Epoch	Visual Classification	P _{PCA}	P _{CaT}	P _{Ti/Fe}
PER451	23:10:43.5	+64:28:52.3	112.349	3.69901	2012	M5.0 III	0.349	0.076	0.169
PER452	23:10:47.7	+64:32:46.5	112.380	3.75635	2012	M3.0 II – III	0.421	0.52	0.177
PER453	23:11:06.0	+57:16:17.8	109.663	-2.99233	2012	M5.0 III	0.38	0.017	0.061
PER454	23:12:22.5	+57:04:44.2	109.751	-3.23579	2012	M4.0 II	0.361	0.684	0.281
PER455	23:12:30.3	+59:58:22.5	110.846	-0.55680	2012	M6.0 II – III	0.474	0.079	0.153
PER456	23:12:42.7	+63:56:10.0	112.344	3.11267	2012	M6.0 III	0.264	0.006	0.099
PER457	23:12:56.1	+59:08:13.5	110.586	-1.35301	2012	M7.5 III	0.268	0.001	0.091
PER458	23:13:13.3	+56:36:12.4	109.681	-3.72023	2012	M8.0 II	0.178	0.0	0.0
PER459	23:13:25.8	+59:36:36.0	110.820	-0.93699	2012	M0.0 Ib	0.772	1.0	1.0
PER460	23:14:37.7	+60:55:16.8	111.439	0.22831	2012	M1.5 Iab	0.866	1.0	1.0
PER461	23:14:42.6	+64:40:05.2	112.816	3.71320	2012	M8.0 III	0.174	0.0	0.043
PER462	23:15:03.6	+59:31:13.7	110.979	-1.09591	2012	M1.5 Iab	0.802	1.0	1.0
PER463	23:15:26.1	+57:27:05.0	110.273	-3.04170	2012	M7.5 II	0.128	0.0	0.211
PER464	23:16:02.0	+62:21:19.0	112.114	1.50429	2011	M5.0 Ib	0.865	0.998	1.0
PER465	23:16:04.5	+57:01:56.9	110.202	-3.46359	2012	M4.0 II	0.346	0.038	0.212
PER466	23:16:29.2	+60:57:45.2	111.664	0.18515	2012	M3.0 Iab	0.854	1.0	1.0
PER467	23:16:47.3	+59:12:31.4	111.072	-1.46605	2012	M3.0 II	0.364	0.989	0.514
PER468	23:17:29.1	+58:40:57.9	110.968	-1.98954	2012	M1.0 Iab – Ib	0.754	1.0	0.998
PER469	23:17:58.4	+62:24:20.4	112.342	1.47120	2012	M4.0 II	0.322	0.84	0.498
PER470	23:18:19.2	+60:16:22.0	111.630	-0.53952	2012	M1.0 Iab – Ib	0.77	1.0	1.0
PER471	23:18:30.4	+58:33:10.8	111.047	-2.15790	2012	M1.0 Ia	0.866	1.0	1.0
PER472	23:18:39.5	+61:53:13.9	112.235	0.95773	2012	K3.0 Ib	0.658	1.0	1.0
PER473	23:18:47.9	+58:07:41.3	110.934	-2.56918	2012	M8.0 III	0.231	0.0	0.029
PER474	23:19:26.7	+58:02:24.2	110.983	-2.68156	2012	M3.5 Ib	0.568	0.106	0.494
PER475	23:19:52.4	+60:47:40.5	111.991	-0.11719	2012	M5.0 III	0.481	0.105	0.223
PER476	23:22:30.7	+59:18:26.0	111.792	-1.62756	2012	M1.0 Ia	0.895	1.0	1.0
PER477	23:23:28.1	+56:10:01.0	110.857	-4.62860	2012	C star	–	–	–
PER478	23:23:39.8	+60:20:00.6	112.272	-0.70893	2012	M1.5 Iab	0.8	1.0	1.0
PER479	23:23:58.4	+55:39:28.6	110.754	-5.13205	2012	S star	0.528	0.997	0.294
PER480	23:24:30.0	+62:14:48.0	113.001	1.06306	2011	M6.0 Ib – II	0.295	0.012	0.081
PER481	23:24:44.8	+61:20:38.4	112.731	0.20110	2012	K3.0 Ib	0.639	1.0	0.999
PER482	23:24:57.2	+62:18:50.8	113.073	1.10942	2012	M4.0 II	0.376	0.239	0.326
PER483	23:25:09.0	+61:22:01.0	112.784	0.20692	2011	M0.5 Iab	0.791	1.0	1.0
PER484	23:25:33.0	+57:49:43.5	111.676	-3.15371	2012	M3.0 Ib – II	0.435	0.929	0.404
PER485	23:26:43.5	+60:23:08.9	112.647	-0.78332	2012	M0.0 Iab	0.766	1.0	1.0
PER486	23:27:38.9	+61:17:27.7	113.043	0.03837	2012	M4.0 II – III	0.373	0.904	0.339
PER487	23:27:51.4	+62:45:37.3	113.533	1.42374	2012	M7.5 III	0.192	0.0	0.002
PER488	23:28:17.8	+57:28:56.9	111.913	-3.59967	2012	C star	–	–	–
PER489	23:29:13.1	+56:39:33.1	111.772	-4.42050	2012	M7.5 Iab	0.349	0.0	0.009
PER490	23:29:29.9	+58:57:11.5	112.526	-2.25306	2012	M5.0 II	0.374	0.02	0.101
PER491	23:30:11.0	+60:16:45.0	113.020	-1.01944	2011	M5.0 Ib	0.764	0.626	0.458
PER492	23:30:44.1	+60:15:20.5	113.078	-1.06284	2012	M4.0 Ib	0.872	0.974	0.878
PER493	23:30:53.0	+62:07:22.0	113.667	0.70878	2011	M0.0 Iab	0.812	1.0	1.0
PER494	23:32:03.1	+59:23:15.1	112.971	-1.94015	2012	M1.0 Ib – II	0.552	1.0	0.956
PER495	23:32:16.4	+61:58:08.3	113.776	0.51274	2012	M0.0 Iab	0.755	1.0	0.998
PER496	23:32:20.8	+62:06:32.2	113.826	0.64363	2012	C star	–	–	–
PER497	23:33:46.5	+61:32:22.6	113.817	0.04992	2012	M1.0 Ib – II	0.539	1.0	1.0
PER498	23:34:21.0	+58:53:05.4	113.102	-2.50786	2012	M9.0 III	0.08	0.0	0.0
PER499	23:35:02.3	+58:34:16.0	113.096	-2.83399	2012	M3.0 Iab	0.897	1.0	1.0
PER500	23:35:27.4	+59:16:18.5	113.351	-2.17925	2012	M1.0 Iab – Ib	0.803	1.0	1.0
PER501	23:35:46.5	+61:07:47.3	113.927	-0.41208	2012	M2.0 II	0.485	0.91	0.265
PER502	23:35:50.4	+58:44:19.0	113.244	-2.70393	2012	M7.0 II	0.226	0.0	0.009
PER503	23:37:20.4	+61:50:14.4	114.308	0.21262	2012	M6.0 II	0.461	0.006	0.048
PER504	23:37:31.2	+59:42:13.5	113.726	-1.84029	2012	K0.0 Ib	0.715	1.0	1.0
PER505	23:38:09.8	+56:01:46.9	112.772	-5.38983	2012	C star	–	–	–
PER506	23:38:23.7	+61:54:20.6	114.446	0.24333	2012	M7.5 II – III	0.242	0.0	0.009
PER507	23:39:19.0	+60:13:02.0	114.085	-1.40990	2011	M2.0 Iab	0.861	1.0	1.0

Table A1: continued.

ID	RA J2000	DEC J2000	l (deg)	b (deg)	Epoch	Visual Classification	P _{PCA}	P _{CaT}	P _{Ti/Fe}
PER508	23:39:35.1	+59:35:09.8	113.944	-2.02597	2012	C star	–	–	–
PER509	23:40:40.6	+65:35:00.5	115.701	3.71005	2012	M3.0 II – III	0.383	0.871	0.251
PER510	23:42:12.3	+65:39:09.1	115.871	3.73428	2012	M2.0 Ib – II	0.706	1.0	0.899
PER511	23:43:06.0	+60:02:47.0	114.493	-1.70096	2011	M8.0 III	0.053	0.0	0.0
PER512	23:43:06.8	+57:52:49.9	113.927	-3.79176	2012	M5.0 II	0.42	0.029	0.143
PER513	23:44:25.0	+59:40:08.0	114.555	-2.10840	2011	M7.0 III	0.2	0.0	0.002
PER514	23:45:05.0	+60:26:51.0	114.835	-1.37687	2011	M4.0 II	0.422	0.987	0.56
PER515	23:45:36.9	+62:20:56.3	115.378	0.44658	2012	M3.0 Ib	0.817	1.0	1.0
PER516	23:45:52.0	+56:55:58.7	114.043	-4.80277	2012	M5.0 III	0.374	0.024	0.168
PER517	23:46:07.0	+60:27:54.0	114.962	-1.39206	2011	M6.5 II	0.339	0.064	0.159
PER518	23:46:11.0	+62:40:05.0	115.521	0.73897	2011	M1.0 Iab – Ib	0.826	1.0	1.0
PER519	23:46:48.1	+60:05:11.6	114.950	-1.77973	2012	M1.0 Iab	0.784	1.0	1.0
PER520	23:47:12.4	+58:54:13.3	114.708	-2.93860	2012	M7.5 II – III	0.112	0.0	0.003
PER521	23:47:21.0	+58:13:16.0	114.557	-3.60476	2011	M6.0 II	0.407	0.003	0.066
PER522	23:47:25.0	+62:24:38.0	115.595	0.45428	2011	M2.0 II	0.446	0.976	0.296
PER523	23:47:41.0	+60:42:37.0	115.209	-1.20199	2011	M5.0 II	0.477	0.009	0.066
PER524	23:47:46.0	+57:42:07.0	114.483	-4.12161	2011	M2.0 II	0.508	1.0	0.644
PER525	23:48:24.0	+58:50:27.0	114.842	-3.03723	2011	M6.0 III	0.323	0.0	0.002
PER526	23:49:19.0	+58:12:00.0	114.804	-3.68804	2011	M5.0 Ib – II	0.287	0.073	0.205
PER527	23:49:38.2	+56:39:25.5	114.477	-5.19673	2012	M1.5 II	0.422	1.0	0.008
PER528	23:50:12.0	+61:06:16.0	115.601	-0.89267	2011	M3.0 Ib	0.826	1.0	1.0
PER529	23:50:43.0	+61:52:33.0	115.841	-0.15713	2011	M2.0 Iab	0.832	1.0	1.0
PER530	23:50:54.3	+65:38:36.9	116.740	3.50222	2012	M2.0 II	0.496	1.0	0.424
PER531	23:51:15.1	+56:50:40.9	114.737	-5.06640	2012	M3.0 II	0.484	0.957	0.149
PER532	23:51:29.0	+62:16:34.0	116.022	0.21148	2011	K3.0 Iab	0.823	1.0	1.0
PER533	23:51:32.0	+57:37:40.0	114.956	-4.31336	2011	M7.0 III	0.173	0.0	0.008
PER534	23:52:04.9	+61:48:12.4	115.982	-0.26469	2012	M9.5 III	0.018	0.0	0.0
PER535	23:56:40.0	+62:11:23.0	116.591	-0.00586	2011	M2.0 Ib	0.805	1.0	1.0
PER536	23:56:44.4	+58:49:01.2	115.889	-3.30480	2012	M7.5 II	0.281	0.0	0.026
PER537	23:56:49.7	+66:05:07.9	117.429	3.79892	2012	M1.0 Ib	0.742	1.0	1.0
PER538	23:57:21.2	+58:25:04.0	115.884	-3.71189	2012	S star	0.187	0.112	0.294
PER539	23:57:44.1	+56:56:46.1	115.627	-5.16196	2012	M4.5 II – III	0.386	0.012	0.075
PER540	23:58:38.0	+60:53:42.0	116.553	-1.32103	2011	M8.0 III	0.061	0.0	0.0
PER541	23:59:05.6	+56:58:15.0	115.814	-5.17573	2012	C star	–	–	–
PER542	3:00:50.60	+58:09:13.7	139.333	-0.53638	2012	M1.0 II	0.536	0.998	0.508
PER543	3:00:50.70	+58:56:29.7	138.958	0.15643	2012	M5.0 Ib – II	0.295	0.019	0.204
PER544	3:03:35.20	+57:52:01.3	139.789	-0.61316	2012	M5.0 III	0.502	0.453	0.29
PER545	3:05:10.40	+59:54:00.3	138.977	1.26157	2012	M6.0 II – III	0.368	0.09	0.143
PER546	3:06:45.00	+55:10:14.3	141.493	-2.74873	2012	M6.5 III	0.28	0.003	0.118
PER547	3:08:44.40	+58:04:37.7	140.280	-0.09321	2012	K3.0 Ib	0.763	1.0	1.0
PER548	3:10:40.80	+54:13:19.9	142.462	-3.28343	2012	M4.5 II	0.545	0.307	0.34
PER549	3:11:12.20	+64:06:57.8	137.474	5.26437	2012	M1.0 Iab	0.809	1.0	1.0
PER550	3:15:03.00	+56:30:30.1	141.815	-1.00436	2012	M1.0 Ib – II	0.549	1.0	0.801
PER551	3:16:30.90	+59:56:00.3	140.184	2.01333	2012	M3.0 II	0.459	0.969	0.454
PER552	3:16:40.80	+58:23:53.2	141.011	0.71959	2012	C star	–	–	–
PER553	3:18:55.10	+54:57:32.8	143.096	-2.03228	2012	M7.0 II	0.26	0.001	0.063
PER554	3:19:07.30	+50:20:12.7	145.605	-5.91882	2012	M3.5 II – III	0.424	0.671	0.223
PER555	3:21:16.70	+54:08:28.5	143.825	-2.53752	2012	K2.0 Ib – II	0.668	1.0	0.999
PER556	3:21:40.60	+52:43:33.6	144.645	-3.69401	2012	M6.0 III	0.244	0.019	0.072
PER557	3:21:59.70	+51:20:29.6	145.442	-4.82854	2012	M4.5 II	0.402	0.23	0.173
PER558	3:22:49.30	+56:01:10.6	142.989	-0.84121	2012	C star	–	–	–
PER559	3:24:13.20	+56:13:33.0	143.039	-0.56191	2012	M4.0 II	0.377	0.725	0.382
PER560	3:24:38.70	+58:22:25.5	141.903	1.26216	2012	M2.0 Ib	0.821	1.0	1.0
PER561	3:28:01.00	+63:49:14.9	139.195	6.00936	2012	M5.0 II	0.298	0.001	0.022
PER562	3:28:08.50	+57:19:26.2	142.874	0.64942	2012	M1.0 Ib	0.702	1.0	1.0
PER563	3:31:22.50	+49:00:58.6	147.999	-5.91299	2012	M5.0 III	0.488	0.225	0.423
PER564	3:31:35.10	+59:33:27.3	141.977	2.74399	2012	M6.5 II	0.329	0.001	0.132

Table A1: continued.

ID	RA J2000	DEC J2000	l (deg)	b (deg)	Epoch	Visual Classification	P _{PCA}	P _{CaT}	P _{Ti/Fe}
PER565	3:32:55.80	+52:44:13.7	146.051	-2.72989	2012	C star	—	—	—
PER566	3:34:29.50	+51:40:36.1	146.862	-3.45532	2012	M6.0 III	0.287	0.0	0.044
PER567	3:39:42.50	+52:08:15.0	147.241	-2.60878	2012	C star	—	—	—
PER568	3:39:50.40	+50:16:43.7	148.370	-4.08685	2012	K5.0 Ib	0.744	1.0	1.0
PER569	3:39:50.70	+51:06:30.3	147.873	-3.42143	2012	M3.0 Ib	0.571	1.0	0.999
PER570	3:40:25.10	+60:46:51.7	142.149	4.37905	2012	M6.0 III	0.336	0.001	0.14
PER571	3:41:48.10	+62:38:54.2	141.150	5.96777	2012	C star	—	—	—
PER572	3:41:56.00	+53:57:10.9	146.419	-0.95553	2012	M4.0 Ib – II	0.437	0.23	0.367
PER573	3:42:49.50	+60:54:08.5	142.310	4.65275	2012	M7.0 II	0.304	0.0	0.04
PER574	3:45:14.30	+55:55:42.9	145.596	0.90206	2012	M0.0 Iab – Ib	0.827	1.0	1.0
PER575	3:45:27.40	+52:10:59.2	147.916	-2.03909	2012	M3.0 II	0.416	0.959	0.708
PER576	3:45:55.70	+60:11:46.6	143.046	4.32734	2012	M6.0 III	0.374	0.007	0.179
PER577	3:47:06.70	+53:03:53.0	147.571	-1.18956	2012	M2.0 Ib	0.624	0.999	0.878
PER578	3:47:07.60	+52:40:41.5	147.812	-1.49219	2012	M3.5 Ib	0.761	1.0	0.96
PER579	3:47:23.50	+54:40:50.0	146.605	0.10657	2012	M1.0 II	0.486	1.0	0.542
PER580	3:47:43.20	+60:06:32.7	143.275	4.39664	2012	M4.5 II	0.285	0.0	0.151
PER581	3:48:40.10	+58:17:11.9	144.506	3.04463	2012	M7.0 II	0.253	0.0	0.017
PER582	3:51:34.00	+56:15:19.0	146.085	1.70624	2011	M4.5 Ib – II	0.394	0.523	0.541
PER583	3:54:06.40	+60:21:00.1	143.741	5.08321	2012	M1.5 Ib – II	0.506	1.0	0.985
PER584	3:58:36.00	+55:41:57.0	147.197	1.90796	2011	M6.5 III	0.223	0.0	0.054
PER585	3:58:38.00	+55:14:27.0	147.499	1.56234	2011	M4.5 Ib – II	0.52	0.155	0.13
PER586	4:03:44.00	+56:34:47.0	147.159	3.04159	2011	M4.0 III	0.461	0.743	0.309
PER587	4:04:21.00	+55:04:20.7	148.225	1.97146	2012	M2.0 Iab	0.855	1.0	1.0
PER588	4:04:27.80	+55:55:26.9	147.671	2.61865	2012	M5.0 II	0.26	0.0	0.021
PER589	4:06:41.10	+58:40:53.2	146.048	4.87007	2012	M4.5 II – III	0.344	0.009	0.203
PER590	4:07:11.60	+55:12:33.3	148.437	2.34465	2012	K4.0 Ib	0.741	1.0	1.0
PER591	4:07:45.40	+60:12:58.5	145.109	6.09537	2012	M5.0 III	0.442	0.297	0.307
PER592	4:10:28.60	+57:51:04.8	146.980	4.59653	2012	M3.0 II	0.396	0.989	0.502
PER593	4:11:26.00	+57:22:29.0	147.400	4.33569	2011	M3.5 II	0.312	0.807	0.687
PER594	4:16:54.30	+57:14:28.0	148.028	4.74939	2012	M0.5 Ib – II	0.535	1.0	0.991

This paper has been typeset from a \LaTeX file prepared by the author.